The Arabidopsis SAC9 Enzyme defines a cortical population of early endosomes and restricts PI(4,5)P 2 to the Plasma Membrane

Mehdi Doumane, Alexis Lebecq, Aurélie Fangain, Vincent Bayle, Frédérique Rozier, Maria del Mar Marquès-Bueno, Romain P Boisseau, Mathilde Laetitia Audrey Simon, Laia Armengot, Yvon Jaillais, et al.

The Arabidopsis SAC9 Enzyme defines a cortical population of early endosomes and restricts PI(4,5)P_2 to the Plasma Membrane

Mehdi Doumane†[1], Alexis Lebecq†[1], Aurélie Fangain[1], Vincent Bayle[1], Frédérique Rozier[1], Maria del Mar Marquès-Bueno[1,3], Romain P. Boisseau[2], Mathilde Laetitia Audrey Simon[1], Laia Armengot[1], Yvon Jaillais[1*], Marie-Cécile Caillaud[1*]

[1] Laboratoire Reproduction et Développement des Plantes, Université de Lyon, ENS de Lyon, CNRS, INRA, F-69342 Lyon, France.

[2] Division of Biological Science, University of Montana, Missoula, MT 59812, USA.

[3] Current address: Department of Molecular Genetics, Center for Research in Agricultural Genomics (CRAG), CSIC-IRTA-UAB-UB, Campus UAB, Bellaterra (Cerdanyola del Vallès), 08193, Barcelona, Spain.

† The authors contributed equally to this work

*Corresponding authors: yvon.jaillais@ens-lyon.fr; marie-cecile.caillaud@ens-lyon.fr

Short title: SAC9 prevents the intracellular accumulation of PI(4,5)P_2 in plant cells.

One-sentence summary: SAC9 prevents the accumulation of PI(4,5)P_2 along the endocytic pathway in plants and thereby contributes to the clathrin mediated endocytosis process at the plasma membrane via its interaction with SH3P2

Keywords: Arabidopsis, endocytosis, phosphoinositides, early endosome, plasma membrane

ABSTRACT ~200 words

Membranes lipids, and especially phosphoinositides, are differentially enriched within the eukaryotic endomembrane system. This generates a landmark code by modulating the properties of each membrane. Phosphatidylinositol 4,5-bisphosphate [PI(4,5)P_2] specifically accumulates at the plasma membrane in yeast, animal and plant cells, where it regulates a wide range of cellular processes including endocytosis. However, the functional consequences of mispatterning PI(4,5)P_2 in plants are unknown. Here, we functionally characterized the phosphoinositide phosphatase *SUPPRESSOR OF ACTIN9* (*SAC9*) in *Arabidopsis thaliana* (Arabidopsis). We found that SAC9 depletion led to the ectopic localization of PI(4,5)P_2 on cortical intracellular compartments, which depends on PI4P and PI(4,5)P_2 production at the plasma membrane. SAC9 localizes to a subpopulation of *trans*-Golgi Network/early endosomes that are spatially restricted to a region close to the cell cortex and that are coated with clathrin. Furthermore, it interacts and colocalizes with the endocytic component Src Homology 3 Domain Protein 2 (SH3P2). In the absence of SAC9, SH3P2 localization is altered and the clathrin mediated endocytosis rate is significantly reduced. Thus, SAC9 is required to maintain efficient endocytic uptake, highlighting the importance of restricting the PI(4,5)P_2 pool at the plasma membrane for the proper regulation of endocytosis in plants.

INTRODUCTION

Phosphoinositides constitute a family of low abundant lipids differentially enriched in the membranes of eukaryotic cells (Platre and Jaillais 2016; Balla 2013; Noack and Jaillais 2020). These versatile lipids can be interconverted into one another. For example, Phosphatidylinositol 4,5-biphosphate [PI(4,5)P_2] is synthetized from Phosphatidylinositol 4-phosphate (PI4P) by PI4P-5 kinases, and is dephosphorylated into PI4P by PI(4,5)P_2 5-phosphatase (Noack and Jaillais 2017). Furthermore, PI(4,5)P_2 and PI4P are targeted by phospholipases C (PLC) into diacylglycerol and soluble phosphorylated inositol (Balla 2013). PI(4,5)P_2 strictly localizes at the plasma membrane in plants and animal cells (van Leeuwen et al. 2007; Carim et al. 2019; Del Signore et al. 2017; Simon et al. 2014; Ben El Kadhi et al. 2011) despite the plasma membrane being constantly turned-over by endocytosis and exocytosis. At the plasma membrane, PI(4,5)P_2 interacts with a variety of extrinsic membrane proteins such as endocytic protein adaptors (Zhang et al. 2015) and actin-regulatory proteins (Paez Valencia et al. 2016), which are recruited and/or activated by the binding to PI(4,5)P_2. Therefore, PI(4,5)P_2 subcellular patterning likely is critical to regulate the recruitment of proteins that act at the plasma membrane, and the cellular processes they mediate, including clathrin-mediated endocytosis.

Consistent with a critical role of PI(4,5)P_2 in the recruitment of the early clathrin-mediated endocytosis factors, a *pip5k1 pip5k2* double mutant in *Arabidopsis thaliana* (Arabidopsis) lacking two ubiquitously expressed PI4P-5 kinases, has abnormal auxin distribution and defective endocytic trafficking of the transmembrane auxin efflux carriers PIN-FORMED 1 (PIN1) and PIN2 (Tejos et al. 2014; Ischebeck et al. 2013; Mei et al. 2012). Furthermore, the *pip5k1 pip5k2* double mutant has an altered dynamic of CLATRHIN LIGHT CHAIN2 (CLC2), with the density of CLC2 foci at the plasma membrane being reduced in the mutant (Ischebeck et al. 2013). Overexpression of Arabidopsis PI4P-5 kinase 6 in tip-growing pollen tubes induced massive aggregation of the plasma membrane in pollen tube tips due to excessive clathrin-dependent membrane invagination, supporting a role for PI(4,5)P_2 in promoting early stages of Clathrin-mediated endocytosis (Zhao et al. 2010). The inducible overexpression of a highly active human PI4P-5 kinase leads to an increase PI(4,5)P_2 production, very strong developmental phenotypes and heightened endocytic trafficking toward the vacuole (Gujas et al. 2017). In addition, we recently showed that inducible depletion of the PI(4,5)P_2 from the plasma membrane using the iDePP system leads to a decrease of the fraction of the clathrin adaptor protein AP2-µ and the Src Homology (SH3)-domain containing protein 2 (SH3P2) at the plasma membrane (Doumane et al. 2021). Furthermore, FM4-64 uptake experiment confirmed an impact of PI(4,5)P_2 depletion from the plasma membrane on bulk endocytic flow.

In animal cells, several PI(4,5)P_2 phosphatases are required for late stages of clathrin-mediated endocytosis (He et al. 2017; Pirruccello et al. 2014). Many PI(4,5)P_2 phosphatases belong to the 5-

Phosphatase enzyme family, including OCRL and synaptojanins (Syn1/2) in animals, and synaptojanin-like proteins (Inp51p/Snjl1p, Inp52p/Sjl2p and Inp53p/Sjl3p) in *Saccharomyces cerevisiae*. The Arabidopsis genome contains 15 genes encoding 5-phosphatases, but only a few are characterized. Mutation in the 5-phosphatases 9 leads to osmotic stress tolerance, with reduced reactive oxygen species production and Ca^{2+} influx (Golani et al. 2013). The 5-phosphatases 6/COTYLEDON VASCULAR PATTERN2 (CVP2) and 5-phosphatases 7/CVP2 LIKE 1 (CVL1) are specifically required for vascular differentiation (Rodriguez-Villalon et al. 2015; Carland and Nelson 2009; Carland and Nelson 2004). Finally,the *5-phosphatases 15/FRAGILE FIBER 3 (FRA3)* is expressed in developing fibers and vascular cells, which is consistent with the defective fiber and vessel phenotypes seen in the loss-of-function *fra3* mutant (Zhong et al. 2004).

Proteins containing SUPPRESSOR OF ACTIN (or Sac1-like) domains constitute another family of phosphoinositide phosphatases (Zhong and Ye 2003). In Arabidopsis, there are nine SAC proteins, forming three clades (Zhong and Ye 2003). The first clade is composed of SAC1, a PI(3,5)P_2 5-phosphatase (Zhong et al. 2005), and its relatives SAC2 to 5, putative PI(3,5)P_2 5-phosphatases (Novakova et al. 2014). The second clade corresponds to SAC7/RHD4 a PI4P 4-phosphatase (Thole et al. 2008) and its relatives SAC6 and SAC8 putative PI4P 4-phosphatases (Song et al. 2021). The third clade is composed of a single member, a plant-specific protein called SAC9. SAC9 has a unique structure, with a SAC phosphoinositide phosphatase domain at its N-terminus, immediately followed by a putative protein/protein interaction domain (WW domain), and a long C-terminal region of 1104 amino acids where no putative domains are predicted by sequence homology analysis (Figure 1A, (Zhong and Ye 2003). The *sac9* mutants is dwarf and it constitutively accumulates anthocyanins and expresses genes from stress response pathways (Williams et al. 2005). Loss-of-function alleles of *SAC9* display a three-fold increase in PI(4,5)P_2 content, together with a decrease of PI4P level, suggesting that it acts as a PI(4,5)P_2 5-phosphatase in planta (Williams et al. 2005).

In this study, we show that the phosphoinositide phosphatase activity of SAC9 is required for its function. Using *in vivo* confocal microscopy, we found that SAC9 localizes in a subpopulation of trans-Golgi network/early endosomes (TGN/EEs) spatially restricted to a region close to the cell cortex. Loss of SAC9 results into PI(4,5)P_2 mis-patterning at the subcellular level, leading to the accumulation of PI(4,5)P_2 in subcortical compartments associated with TGN/EEs. SAC9 interacts and colocalizes with the endocytic component SH3P2. In the absence of SAC9, and therefore when the patterning of the PI(4,5)P_2 is compromised, SH3P2 localization is affected and the CLC dynamics is significantly reduced. Thus, SAC9 is required to maintain efficient endocytic uptake, highlighting the importance of restricting the PI(4,5)P_2 pool to the plasma membrane for proper endocytosis in plants.

RESULTS

The cysteine 459 in the catalytic domain of SAC9 is required for its function

We investigated the root phenotype in the already described mutant alleles of SAC9 (Vollmer et al. 2011; Williams et al. 2005). As previously described, *sac9-1*$^{-/-}$ and *sac9-3*$^{-/-}$ knock-out mutants are two times shorter compared to the Wild-type (WT) Col-0, at 12 days post-germination (dpg; Figure 1B and 1C). We also observed a three-time decrease in the lateral root density of *sac9-1*$^{-/-}$ and *sac9-3*$^{-/-}$ compared to WT plants (Figure 1B to 1D). To confirm that the phenotype observed was due to the loss-of-function of SAC9, we generated Arabidopsis lines expressing SAC9 fused to a fluorescent protein (mCIT-SAC9 and TdTOM-SAC9) under SAC9 native promoter (*SAC9pro)* or the *UBIQUITIN10* promoter (*UBQ10pro*), respectively (Figure 1). To assess the biological relevance of SAC9 phosphatase activity, we also generated a mutated version of SAC9 in the C459 catalytic cysteine into an Alanine (mCIT-SAC9^{C459A}) from C-x(5)-R-[T/S] conserved catalytic motif in the SAC domain (Hsu and Mao, 2015, 2013, Figure 1 and Supplemental Figure 1A). We found that both *SAC9pro:mCIT-SAC9* and *UBQ10pro:TdTOM-SAC9* rescued *sac9-3*$^{-/-}$ mutant root phenotype while *SAC9pro:mCIT-SAC9*^{C459A} did not, indicating that i) the root phenotypes described above are indeed caused by *SAC9* loss-of-function, ii) N-terminally tagged SAC9 proteins are functional, and iii) SAC9 phosphatase activity is required for SAC9 function (Figure 1B to 1D).

SAC9 localizes to a population of early endosomes close to the plasma membrane

Some phosphoinositide-phosphatases such as Metazoan Sac1 and yeast Sac1p, are able to dephosphorylate *in vitro* several phosphoinositide species, but display a narrower specificity *in vivo* (Hughes et al. 2000; Guo et al. 1999; Rivas et al. 1999). Also, some enzymes involved in phosphoinositide metabolism, such as the yeast PI 4-kinases Stt4p and Pik1p, specifically impact distinct pools of a given phosphoinositide species depending on their subcellular localization (Roy and Levine 2004; Yoshida et al. 1994; Flanagan et al. 1993). Using stable transgenic lines expressing the functional *SAC9pro:mCIT-SAC9* and *Ub10pro:TdTOM-SAC9* constructs, we assessed the subcellular distribution of SAC9 in rescued *sac9-3*$^{-/-}$ homozygous plant using live-cell fluorescence imaging. In meristematic epidermal cells of Arabidopsis roots, mCIT-SAC9 and TdTOM-SAC9 were mainly soluble and excluded from the nucleus (Supplemental Figure 1B). At the cortex of the cell, in close vicinity to the plasma membrane, mCIT-SAC9 localized to a cortical population of mobile dotty structures (Figure 2A, 2B Supplemental Movie 1). We observed that mCIT-SAC9^{C459A} was less soluble with a three-fold increase in the number of mCIT-SAC9^{C459A} labeled dotty structures compared with the signal collected for the functional fusion proteins mCIT-SAC9 and TdTOM-SAC9 (Figure 2C to

2E). This result suggests that the phosphoinositide phosphatase activity is required for the dynamic interaction of SAC9 with intracellular membranes. Co-visualization of TdTOM-SAC9 and mCIT-SAC9^{C459A} (Figure 2F) in Col-0 background demonstrated that all TdTOM-SAC9 dotty structures colocalized with mCIT-SAC9^{C459A} at the cortex of the cell, indicating that the catalytic activity of SAC9 is only partially required for SAC9 localization. When imaging cells in their cortical part close to the plasma membrane, the mCIT-SAC9^{C459A} signal was concentrated in intracellular compartments at the close vicinity with the plasma membrane labelled by the hydrophobic protein Lti6b-2xmCH (Figure 2G). These results suggest a function for SAC9 in regulating phosphoinositide homeostasis either at or in the close vicinity of the plasma membrane.

We next investigated the nature of the intracellular structures labeled by mCIT-SAC9. Both mCIT-SAC9 and mCIT-SAC9^{C459A} colocalized with the amphiphilic styryl dye (FM4-64) stained endosomal compartments at the cell's cortex, just beneath the plasma membrane (Figure 3A and 3B). We observed that Brefeldin A (BFA) treatment led to the aggregation of mCIT-SAC9 and mCIT-SAC9^{C459A} into BFA bodies (Figure 3C and 3D). Since early endosomes/TGN (EE/TGN) are sensitive to BFA while late endosomes (LE/MVB) are not (Takagi and Uemura 2018), this result suggest that both functional and catalytically dead SAC9 fusion proteins localize to endosomes and are likely part of the early steps of endocytic trafficking pathway.

To get more precise insights into the SAC9's localization at the TGN, we crossed Arabidopsis lines expressing fluorescent tagged SAC9 and SAC9^{C459A} proteins with endomembranes markers (Geldner et al. 2009). Using live-cell imaging in root meristematic cells, we observed that mCIT-SAC9 colocalized with TGN markers (CLC2-RFP >79% colocalization; mCH-RabA1g >91%, mCH-VTI12$^{126-222}$ >67%; Figure 3C, 3E and 3F). The colocalization of mCIT-SAC9 with these TGN markers was only partial since mCIT-SAC9 was predominantly observed in the cortical section of the cell (Figure 2A), at the close vicinity to the plasma membrane, whereas classical TGN markers are not restricted to the cell cortex (Figure 3E and 3F). This was even more striking when localizing the fluorescent tagged SAC9 together with mCH-RabD1 (<26% colocalization, Figure 3E and 3F) that also localizes at TGN. Eventually, mCIT-SAC9 showed very weak colocalization with late endosome (LE/MVB) marker (mCH-RabF2a <17%, Figure 3E and 2F), and with the Golgi marker (mCH-Got1p <1%, Figure 3E and 3F). Similarly, mCIT-SAC9^{C459A} strongly colocalized with CLC2-RFP and mCH-RAB-A1g markers, whereas it colocalized much weakly with mCH-RabD1 and did not colocalized with the Golgi marker (Figure 3C, 3G and 3H). This confirmed that SAC9 and SAC9^{C459A} fusion proteins localized to the TGN/EE, with the noticeable difference that SAC9 localization in endomembrane compartments was restricted to the cortex of the cell, suggesting a role of SAC9 in PI(4,5)P_2 homeostasis between the plasma membrane and early endosomal compartments.

SAC9 is required to maintain the pool of PI(4,5)P_2 at the plasma membrane

It was previously reported that Arabidopsis *sac9-1* loss-of-function mutant had a diminution of PI4P and a three-fold accumulation of PI(4,5)P_2, suggesting that SAC9 has a PI(4,5)P_2 5-phosphatase catalytic activity (Williams et al. 2005). In order to visualize the effect of the perturbation of the PIP-metabolism in the absence of SAC9, we introgressed two independents PI(4,5)P_2 biosensors (Simon et al. 2014) into *sac9-3*$^{-/-}$ genetic background. As expected, both PI(4,5)P_2 biosensors strictly labeled the plasma membrane in wild-type cells (Figure 4A and 4C). In *sac9-3*$^{-/-}$, mCIT-2xPH^{PLC} and mCIT-TUBBYc not only labeled the plasma membrane, but also decorated cortical intracellular dotty structures (Figure 4A and 4C). Thus, SAC9 is required for PI(4,5)P_2 restriction at the plasma membrane. We also observed an increase of the number of intracellular compartments labeled by the PI4P biosensors (Simon et al. 2014; Simon et al. 2016) mCIT-PH^{FAPP1} and mCIT-P4M^{SidM}, but not for mCIT-PH^{OSBP} (Figure 4B and 4C). These results is consistent with a diminution of the PI4P pool at the plasma membrane and therefore the relocalization of the PI4P biosensor at intracellular compartments, as previously reported (Simon et al. 2016). The subcellular localization of PI3P sensors (mCIT-FYVE^{HRS} and mCIT-PHOX^{p40}) was identical between Col-0 and *sac9*$^{-/-}$ cells (Figure 4C, Supplemental Figure 2A). We also detected a slight but significant decrease in the density of intracellular compartments decorated by mCIT-C2^{Lact} phosphatidylserine biosensor in *sac9-3*$^{-/-}$ (Figure 4C; Supplemental Figure 2B). Taken together, these results indicate that SAC9-depletion leads to a massive change in PI(4,5)P_2 subcellular patterning, which is present on intracellular cortical structures instead of only being present at the plasma membrane.

Previous investigation of the fine structure in *SAC9* mutant allele reported a massive accumulation of vesicles, presumably containing cell wall, at the close vicinity to the plasma membrane (Vollmer et al. 2011). When co-imaging 2xmCH-2xPH^{FAPP1} together mCIT-TUBBYc in *sac9-3*$^{-/-}$ (Figure 4D), the dotty structures decorated by the PI(4,5)P_2 biosensor —but not with the PI4P biosensor— were observed at the cortex of the cell, at the close vicinity with the plasma membrane (Figure 4D upper panel and 4E), whereas those structures were rarely observed in the internal part of the cell (Figure 4D lower panel and 4E). Therefore dotty structures containing PI(4,5)P_2 were associated with PI4P labelled complements but they did not strictly overlap. Confocal imaging of *sac9-3*$^{-/-}$ mutant co-expressing mCIT-TUBBYc with endosomal markers revealed that the dotty structures containing PI(4,5)P_2 were found associated with FM4-64 endocytic tracer as well as TGN markers (Supplemental Figure 3A-B). Furthermore, BFA treatment efficiently induced 2xmCH-2xPH^{FAPP1} positive BFA bodies in *sac9-3*$^{-/-}$ but did not affect the distribution of mCIT-TUBBYc compartments in the same cells (Supplemental Figure 3C). Therefore, PI(4,5)P_2 intracellular compartments in *sac9-3*$^{-/-}$ are devoid of any ARF GTPase activated by BFA sensitive ARF-GEF. *In vivo* time-lapse imaging of PI(4,5)P_2 biosensor mCIT-TUBBYc and mCIT-2xPH^{PLC} in *sac9-3*$^{-/-}$ mutant revealed that those intracellular structures were mobile

in the cortex of root epidermal cells, hence, behaving like intracellular compartments (Supplemental Figure 3D, Supplemental movie 2).

We next addressed the turnover and the origin of the cortical intracellular PI(4,5)P_2 compartment observed in *sac9-3*$^{-/-}$. We previously showed that short-term treatment (15-30 min) with phenyl arsine oxide (PAO), a pan PI 4-kinases inhibitor, significantly depletes PI4P (Figure 5E) but not PI(4,5)P_2 pools at the plasma membrane of plant cells, whereas longer treatment (> 60 min) affects the synthesis of both lipids (Figure 5A, Platre et al., 2018; Simon et al., 2016). We used this pharmacological approach to test the effect of the inhibition of either PI4P, or both PI4P and PI(4,5)P_2 synthesis, on *sac9-3*$^{-/-}$ anomalous PI(4,5)P_2 intracellular compartments (Figure 5B to 5E). Solubilization of mCIT-PH$^{FAPP1-E50A}$ PI4P biosensor in *sac9-3*$^{-/-}$ cells treated for either 30 or 120 min with PAO confirmed the efficient PI4P depletion in both conditions (Figure 5E). Solubilization of mCIT-TUBBYc PI(4,5)P_2 biosensor in WT after 120 min of PAO exposure, but not after 30 min, confirmed that an efficient PI(4,5)P_2 depletion occurred only for the longest treatment (Figure 5B and 5C). 30 min PAO treatment did not affect anomalous *sac9-3*$^{-/-}$ PI(4,5)P_2 compartments, but 120 min PAO treatment significantly reduced the number of anomalous PI(4,5)P_2 compartments compared to both 120 min mock treatments or 30 min short treatment (Figure 5B and 5C), showing that intracellular PI(4,5)P_2 compartments in *sac9-3*$^{-/-}$ are dependent on the PI4P synthesis, itself substrate for PI(4,5)P_2 production.

SAC9 is required for efficient endocytic trafficking

Because of the specific localization of SAC9 at the cortex of the cell and its colocalization with early TGN/EE markers, we wondered whether PI(4,5)P_2 defective patterning in *sac9-3*$^{-/-}$ correlated with endocytic defects. We counted the number of labeled endosomes following FM4-64 endocytic tracer treatment in cells from WT and *sac9-3*$^{-/-}$ seedlings (Rigal et al. 2015). We observed a significant near two-fold decrease in the number of FM4-64-labelled endosomes per cells in *sac9-3*$^{-/-}$ compared to WT (Figure 6A and B), that was not caused by smaller cells in *sac9-3*$^{-/-}$ as the density of FM4-64-labelled endosomes was also strongly and significantly decreased compared to WT (Supplemental Figure 4).We inhibited recycling with BFA, and used FM4-64 tracer to monitor the endocytosis by measuring the number of BFA bodies labeled by FM4-64 in Col-0 and *sac9-3*$^{-/-}$. We observed significantly less FM4-64-labelled BFA bodies per cells in *sac9-3*$^{-/-}$ compared to wild-type (Figure 6C and D), confirming the lower rate of endocytosis in this mutant. We then assessed whether SAC9 depletion affected the trafficking of cargo proteins. We, therefore, performed another BFA assay, but using the integral membrane protein PIN-FORMED2 fused with GFP (PIN2-GFP) which localizes at the plasma membrane and in intracellular organelles as it continuously recycles (Armengot et al. 2016). We observed significantly less PIN2-GFP-labelled BFA bodies per cell in *sac9-3*$^{-/-}$ compared to WT (Figure

6E and F). PIN2-GFP being partially located on intracellular organelles before BFA treatment, the effect observed may, therefore, indicate an endocytic defect as supported by the others experiments, , and/or a more general defect in trafficking in *sac9-3*$^{-/-}$.

To gain further insights into the function of SAC9 in bulk endocytosis, we investigated the sensitivity of the *sac9* mutant to pharmacological inhibition of endocytosis. To this end, we used the recently described ES9-17, which is a specific inhibitor of clathrin-mediated endocytosis (Dejonghe et al. 2019). We treated wild-type and *sac9-3*$^{-/-}$ seedlings with ES9-17 for 180 min and labeled the plasma membrane and endosomes with FM4-64. Cells from both mock-treated wild-type and *sac9-3*$^{-/-}$ seedlings did not display any obvious defect (Figure 6G). On the contrary, we observed dome-shaped plasma membrane invaginations in ES9-17 long-term treatment of Col-0 seedlings, almost exclusively in elongating or differentiated cells (epidermal or root cap cells), substantiating the possibility that these invaginations constitute read-outs of long term disturb endocytosis (Figure 6G and H). Strikingly, we observed a much higher number of dome-shaped plasma membrane invagination in cells from ES9-17 treated *sac9-3*$^{-/-}$ (Figure 6G and H), showing that SAC9 depletion causes over-sensitivity to inhibition of endocytosis. Hypersensitivity to endocytosis inhibition, decreased internalization of the bulk endocytic tracer FM4-64 and defects in PIN2 protein trafficking together indicate that endocytic trafficking is impacted in the absence of SAC9.

SAC9 is required for SH3P2 localization at the plasma membrane.

To gain some insights into SAC9 function, we next screened for SAC9 interactors using a yeast two hybrid assay against a universal Arabidopsis normalized dT library (ULTImate Y2H SCREEN, hybrigenics). As a bait, we used a portion of SAC9 (AA 499 to 966), which includes the WW domain, a putative protein-protein interaction platform. Out of 59.6 million screened interaction, we recovered and sequenced 260 independent clones corresponding to 107 different proteins. However, among these proteins, most were classified as proven artifact or low confidence interaction and only three candidates (2.8 %) were ranked as very high confidence in the interaction (Supplemental Table 2). Among the high confident interaction candidate, we identified 11 clones corresponding to SH3P2 (5 independent clones). In the yeast-two-hybrid screen, the selected interaction domain identified for SH3P2, corresponds to the C-terminal part of the proteins (aa 213-368), which includes the SH3 domain (Figure 7A). We decided to focus on this candidate because, like SAC9, SH3P2 is linked to both clathrin-mediated endocytosis and membrane phosphoinositides. Indeed, SH3P2 i) colocalizes with clathrin light chain, ii) cofractionates with clathrin-coated vesicles (Nagel et al. 2017), and iii) co-immunoprecipitates in planta with clathrin heavy chain (Nagel et al. 2017), clathrin light chain (Adamowski et al. 2018) and the dynamin DRP1A (Ahn et al. 2017). Furthermore, SH3P2 binds to

various phosphoinositides in vitro (Zhuang et al. 2013; Ahn et al. 2017), and its plasma membrane localization is dependent on PI(4,5)P_2 in vivo (Doumane et al. 2021).

Using live cell imaging we observed that fluorescently tagged SAC9^{C459A} and SH3P2 colocalized in a subcortical population of endomembrane compartments (Figure 7BC), probably TGN/EEs (Figure 3E and F). Because SH3P2 was described to play a role at different steps of the trafficking, from the endocytosis at the plasma membrane to autophagy, we next addressed more precisely which pool of SH3P2 was affected in absence of SAC9. Using confocal imaging, we observed a diminution of the signal corresponding to SH3P2-sGFP at the plasma membrane compared to the cytoplasm in *sac9* (Figure 7D-E). Thus, consistently with the idea that SAC9 regulates SH3P2 localization at the plasma membrane through its interaction, these results point toward a role of SAC9 in endocytosis.

The endocytic protein T-PLATE has an altered dynamic in the absence of SAC9

SAC9 is observed at the close vicinity to the plasma membrane and its absence causes a mislocalization of its protein partner SH3P2, as well as a reduction of the overall endocytosis process. We then assessed if the clathrin-mediated endocytosis at the plasma membrane was affected in absence of SAC9. Using Total Internal Reflection Fluorescence (TIRF) microscopy, we determined the density and dynamic behavior of the endocytic protein from the T-PLATE complex, T-PLATE-GFP, in the *sac9* mutant compared with wild-type plants. Quantitative analysis revealed that the density of T-PLATE-GFP was reduced in sac9-3$^{-/-}$ compared with the WT (Figure 8A, B; supplemental movie 3). Analysis of the dynamics of T-PLATE-GFP at the plasma membrane of etiolated hypocotyl revealed a decrease of the dwell time of T-PLATE-GFP at the plasma membrane in the *sac9* mutant compared to the WT. This result is in line with a reduction of the endocytic flow in the absence of SAC9, and suggests that maintaining a strict plasma membrane accumulation of PI(4,5)P_2 is critical for clathrin-mediated endocytosis.

DISCUSSION

Here, we showed that the phosphatase activity of SAC9 is required for its function, and that fluorescent SAC9 protein fusions colocalize with TGN/EE markers in a subpopulation of endosomes close to the plasma membrane. We found that the subcellular patterning of PI(4,5)P_2 is defective in *sac9* mutants, consistent with the idea that SAC9 is a PI(4,5)P_2 5-phosphatase. In planta, SAC9 interacts and colocalizes with the endocytosis component SH3P2. In the absence of SAC9, and therefore when the patterning of the PI(4,5)P_2 at the plasma membrane and at its close vicinity is affected, SH3P2 no longer localizes at the plasma membrane and the rate of clathrin-mediated endocytosis is significantly reduced. Together, these findings underlie the importance of strictly restricting PI(4,5)P_2 to the plasma membrane during the endocytic process.

SAC9 and phosphoinositide interconversion along the endocytic pathway

In animal cells, a phosphoinositide conversion cascade has been described through the successive action of phosphoinositide kinases and phosphatases. This cascade starts with PI(4,5)P_2 at the plasma membrane and ends-up with PI3P in the membrane of early endosomes (Noack and Jaillais 2017; Schmid and Mettlen 2013; Abad et al. 2017; Posor et al. 2015; Posor et al. 2013; Shin et al. 2005). Briefly, PI(4,5)P_2 is dephosphorylated at the plasma membrane or during the endocytic process by 5-phosphatase enzymes such as OCRL and synaptojanin (De Matteis et al. 2017) (Cauvin et al. 2016; Nandez et al. 2014; Ben El Kadhi et al. 2011; Posor et al. 2013). PI4P is then phosphorylated into PI(3,4)P_2 inside clathrin-coated pits by a PI3-Kinase (PI3K C2α), before being converted into PI3P through the action of a PI4P phosphatase on clathrin-coated vesicles (Schmid and Mettlen 2013; Posor et al. 2013). Because both PI(4,5)P_2 and PI3P are essential regulators of endocytic trafficking, this conversion cascade, and in particular the precise recruitment of dedicated enzymes at the right place and at the right time during endocytosis, is of critical importance of clathrin-mediated endocytosis to proceed normally (Noack and Jaillais 2017; Schmid and Mettlen 2013).

Plants have a much simpler endosomal system, where the TGN functions as an early endosome. This hybrid compartment collects endocytic vesicles and redirects cargo proteins either to the plasma membrane for recycling or to late endosomes/vacuole for degradation (Dettmer et al. 2006; Narasimhan et al. 2020; Rodriguez-Furlan et al. 2019). The plant TGN/EE is enriched in PI4P, not PI3P, which instead accumulates in late endosomes (Noack and Jaillais 2020; Simon et al. 2014). Interestingly, we found that i) SAC9 localizes to clathrin-coated vesicles close to the plasma membrane, and ii) the *sac9* mutant accumulates PI(4,5)P_2 in vesicular structures at the cortex of the cells. Together, we propose that SAC9 represent the long sought-after enzyme which performs the PI(4,5)P_2-to-PI4P conversion

during the plant endocytic process (Figure 9). As such, SAC9 is required to erase PI(4,5)P_2 in endosomal membranes and thereby maintains this lipid strictly at the plasma membrane.

Accumulation of PI(4,5)P_2-containing vesicles in the *sac9* mutant

In the absence of SAC9, PI(4,5)P_2 accumulates inside the cell in what appears to be abnormal compartments that are associated with but independent from TGN/EEs. We can speculate that the prolonged accumulation of PI(4,5)P_2 on clathrin-coated vesicles, and perhaps the lack of PI4P production on these structures, impairs the function of these vesicles. Ultrastructural analyses previously revealed that *sac9* accumulates extra vesicles close to the cell surface (Vollmer et al. 2011). The finding of these unknown subcortical vesicles in *sac9* resonates with our confocal microscopy observations of ectopic PI(4,5)P_2-containing vesicles in this mutant. Importantly, we found that these vesicles are not extensively labeled after a short-term FM4-64 treatment. This suggests that these vesicles are accumulating slowly over time in the *sac9* mutants and are not actively exchanging membrane materials with the TGN/EEs or the plasma membrane, at least not in the 30-minute time frame of the FM4-64 pulse labeling experiment. Together, we propose that PI(4,5)P_2 accumulation on endocytic vesicles after scission could lead to an altered dynamics of these vesicles, which may be unable to fuse correctly with TGN/EEs, ultimately leading to their accumulation in the cell cortex (Figure 9).

We observed that the endocytic pathway is partially impaired in absence of SAC9, and that *sac9* was oversensitive to ES9-17-mediated inhibition of endocytosis. In animal cells, membrane protuberances have been reported in cultured cells knocked-out or knock-down for enzymes of PI(4,5)P_2 metabolism (Gurung et al. 2003; Terebiznik et al. 2002; Mochizuki and Takenawa 1999). These protuberances could therefore be a conserved process affected by disturbed PI(4,5)P_2 homeostasis in both plant and animal cells leading to such plasma membrane distortion. It is not the first observation of plasma membrane protuberances in cells where PI(4,5)P_2 homeostasis is affected: upon PIP5K6 over-expression in pollen tubes, which increases PI(4,5)P_2 levels, plasma membrane invaginations also occurs. The authors elegantly demonstrated that these plasma membrane distortions are due to clathrin-mediated endocytosis defects (Zhao et al. 2010). These structures were also reported when inducible depletion of PI(4,5)P_2 at the plasma membrane of root cells was performed using the iDePP system (Doumane et al. 2021), suggesting that the tight regulation of the PI(4,5)P_2 metabolism is important for the integrity of the plasma membrane. Previous study on the cellular organization of the primary roots of *sac9-1* seedlings at ultrastructural level reported the excessive membrane material either in direct contacts or close to the wall forming the protuberances (Vollmer et al. 2011). The irregular cell wall deposition in the *sac9* mutant leads to cell wall ingrowths, coined “whorl-like structures” (Vollmer et al. 2011). We

propose that such protuberances could be a readout of long-term endocytic defects, for instance caused by an excess of plasma membrane due to unbalanced exocytosis. If so, the appearance of plasma membrane protuberances upon PI(4,5)P_2 metabolism perturbation could be an additional indication of disturbed endocytosis.

How could SAC9 regulate endocytosis?

We observed that the endocytic pathway is partially impaired in the absence of SAC9. We envision several scenarios to explain these endocytic defects. They are not mutually exclusive and ultimately, it would not be surprising if the *sac9* endocytic phenotype results from a combination of altered cellular pathways relying, directly or indirectly, on the precise spatio-temporal regulation of anionic lipid homeostasis. First, as mentioned in the paragraph above, the *sac9* mutant likely accumulates ectopic vesicle following endocytosis. These vesicles trap membrane components inside the cell, which may overall impact the endocytic process. In addition, it is possible that the localization or dynamics of PI(4,5)P_2 binding proteins, which regulate clathrin-mediated endocytosis, could be impacted, as we observed for SH3P2 and T-PLATE (Zhuang et al. 2013; Yperman et al. 2021b; Yperman et al. 2021a). Other proteins from the T-PLATE complex also interact with anionic lipids, including PI(4,5)P_2, and could be affected in *sac9* (Yperman et al. 2021b; Yperman et al. 2021a). Furthermore, the dynamics of dynamin-related proteins, which contain a lipid-binding plekstrin homology domain, and the AP2 adaptor complex, which relies on PI(4,5)P_2 for localization in planta (Doumane et al. 2021), could also be altered in *sac9*. It was also recently reported that perturbation of clathrin-containing vesicles at the TGN/EEs also impacts clathrin-mediated endocytosis (and conversely) (Yan et al. 2021). It is thus possible that perturbing phosphoinositides metabolism after the scission of clathrin-coated vesicles from the plasma membrane impacts the dynamics of clathrin-mediated endocytosis at the cell surface in an indirect way, for example because of slowed recycling of the clathrin pool or other endocytic components at the surface of TGN/EEs.

It is also important to note that bulk endocytosis in general and clathrin-mediated endocytosis in particular are still going-on in the *sac9* mutant, albeit at a reduced rate. Thus, while PI(4,5)P_2 strict exclusion from intracellular membranes is important for the endocytic process, the plant membrane trafficking system appears to be extremely resilient, as it manages to operate despite the accumulation of these membrane of mixed identity inside the cell. Here, we can speculate that SAC9 may not be the only 5-phosphatase enzyme that can control PI(4,5)P_2 homeostasis during endocytosis. In addition, while PI(4,5)P_2 is the main phosphoinositide regulating the recruitment of endocytic regulators in animals, it is likely not the case in plants. Indeed, PI4P, not PI(4,5)P_2, is the major anionic lipids that powers the plasma membrane electrostatic field (Simon et al. 2016), and is very likely key to recruit

385 endocytic proteins in plants (Yperman et al. 2021b; Yperman et al. 2021a). In addition, phosphatidic
386 acid (PA) is also important to drive the electrostatic field of the plasma membrane (Platre et al. 2018)
387 and PA could be involved in the localization of AtEH1/Pan1, a component of the T-PLATE complex
388 (Yperman et al. 2021a).

389

390 **Limitation of the study**

391 SAC9 was previously proposed to act as a PI(4,5)P_2 5-phosphatase in planta, mainly because the
392 *sac9* mutant accumulates PI(4,5)P_2 (Williams et al. 2005). We found an accumulation of PI(4,5)P_2
393 sensors inside the cells in *sac9*, which is fully consistent for a 5-phosphatase enzyme. However, we
394 could not confirm this activity in vitro. This is mainly due to problems in purifying SAC9 catalytic
395 domain in sufficient quantity. Yet, it represents a weakness of our study that we should keep in mind.
396 Indeed, although this is not the most parsimonious explanation, it is possible that SAC9 is not a 5-
397 phosphatase and that instead it controls the localization or activity of another enzyme bearing this
398 catalytic activity. Nonetheless, the fact that catalytically inactive mCIT-SAC9^{C459A} fusion protein does
399 not rescue *sac9* macroscopic phenotype suggests that SAC9 phosphatase activity is required for its
400 function.

401 To explain the endocytic defects observed in the *sac9* mutant, we mainly focused on PI(4,5)P_2 mis-
402 patterning. However, biochemical measurements also showed that the *sac9* mutant accumulates less
403 PI4P than its wild-type counterpart. Given the importance of PI4P for plant cell function (Noack et al.
404 2020; Simon et al. 2016), it is possible that PI4P rather than (or in combination with) PI(4,5)P_2 defects
405 are involved in the *sac9* phenotypes. Given that phosphoinositide metabolism is highly intricate, we
406 fully recognize that it is difficult to fully untangle the specific involvement of each lipid in the observed
407 phenotypes. In addition, the SAC9 protein may carry specific functions outside of its catalytic activity.
408 For example, SAC9 directly interacts with SH3P2, yet the physiological relevance of this interaction
409 for both SAC9 and SH3P2 function remains unclear. Structure-function analyses aiming at dissecting
410 this interaction will be instrumental to clarify this point. In addition, the exact function of SH3P2 in
411 endocytosis is also elusive and it will be important to analyze it in details in the future. Finally, one of
412 the clear limitations in interpreting the *sac9* phenotype, which is common to most genetic approaches,
413 is the accumulation of defects over a long-time period in the mutant. As such, it is impossible to pin-
414 point toward direct or indirect effects of PI(4,5)P_2 mis-patterning on the cellular and developmental
415 phenotypes of this mutant. Future studies, aiming at rapidly manipulating SAC9 function and
416 localization in an inducible manner will be instrumental in disentangling the direct and indirect effects
417 of SAC9 on lipid dynamics and endocytosis regulation.

MATERIALS AND METHODS

Growth condition and plant materials

Arabidopsis thaliana Columbia-0 (Col-0) accession was used as wild-type (WT) reference genomic background throughout this study. Arabidopsis seedlings *in vitro* on half Murashige and Skoog (½ MS) basal medium supplemented with 0.8% plant agar (pH 5.7) in continuous light conditions at 21 °C. Plants were grown in soil under long-day conditions at 21 °C and 70% humidity 16 h daylight.

Cloning

SAC9 promoter *(SAC9pro*; 800 bp) was amplified from Col-0 genomic DNA using *SAC9prom_fwd_gb* TTGTATAGAAAAGTTGCTATTGAAAAAAGATAGAGGCGCGTG and *SAC9prom_rev_gb* TTTTTTGTACAAACTTGCCTGAGCTCAGGACCAAGCGG primers and the corresponding PCR product was recombined into *pDONR-P1RP4* (life technologies www.lifetechnologies.com/) vector by BP reaction to give *SAC9pro/pDONR-P1RP4*. The *mCIT* and *TdTOM* containing vectors *cYFPnoSTOP/pDONR221* and *TdTOMnoSTOP/pDONR221* were described before (Simon et al., 2014; Jaillais et al., 2011).

The genomic sequence of *SAC9* (At3g59770) was amplified by PCR using 7-day old Arabidopsis seedlings gDNA as template and the *SAC9-B2R* GGGGACAGCTTTCTTGTACAAAGTGGCTATGGATCTGCATCCACCAGGTTAGT and *SAC9-B3wSTOP* GGGGACAACTTTGTATAATAAAGTTGCTCAGACACTTGAAAGGCTAGTCCAT primers. The corresponding PCR product was recombined into *pDONR-P2RP3* vector by BP reaction to give *SAC9g/pDONR-P2RP3*.

SAC9^{C459A} mutation was obtained by site-directed mutagenesis using the partially overlapping SAC9-C459A-F TACGTTTTAACGCTGCTGATTCCTTGGATCGAACAAATGC and SAC9-C459A-R AGGAATCAGCAGCGTTAAAACGTATCACCCCATTTTGATGTG primers on *SAC9g/pDONR-P2RP3*.

Final destination vectors were obtained using three fragments LR recombination system (life technologies, www.lifetechnologies.com/) using pB7m34GW destination vector (Karimi et al. 2007). The following reactions were set-up to generate the corresponding destination vectors: UBQ10prom:tdTOM-SAC9g/pH, SAC9prom:mCIT-SAC9g/pB, pAtSAC9:mCIT-SAC9g^{DEAD}/pB, SAC9prom:TdTOM-SAC9g^{DEAD}/pH (Supplemental Table 1).

FM4-64 staining and drug treatments

Seedlings were incubated in wells containing 1 µM FM4-64 (Life Technologies T-3166; from a stock solution of 1.645 mM = 1 mg/ml in DMSO) in half Murashige and Skoog (½ MS) liquid basal medium without shaking for 30 min and in dark. Seedlings were then mounted in the same medium and imaged within a 10 min time frame window (1 h ± 5 min).

Seedlings were incubated in wells containing Brefeldin A (BFA; Sigma B7651) applied at 50 µM (from a stock solution of 30 mM in DMSO), or a corresponding volume of DMSO as 'mock' treatment, dissolved in liquid ½ MS for one hour in dark without shaking before mounting in the same medium and imaging. For co-treatment with 50 µM BFA and 1 µM FM4-64, FM4-64 and BFA were added at the same time. Imaging was performed within a 14 min time frame window (1 h ± 7 min).

For PAO treatment, seedlings were incubated in wells containing 30 µM PAO (Sigma P3075, www.sigmaaldrich.com, PAO stock solution at 60 mM in DMSO), or a volume of DMSO as mock treatment, during the indicated time. Roots were imaged within a 10 min time frame window around the indicated time. The PAO effects on the localization of our biosensors were analyzed by counting manually the number of labelled compartments per cell.

ES9-17 was stored at -20°C as a 30 mM stock solution in DMSO. Seedlings were incubated in dark without shaking for the indicated duration (± 7 min) in liquid ¼ MS (pH 5.7) in wells containing 1 % DMSO to help solubilization of ES9-17, and either 1 µM ES9-17 or the corresponding additional volume of DMSO (mock treatment). For 1 µM ES9-17 and 1 µM FM4-64, FM4-64 was added 30 min after the ES9-17 (the indicated time corresponds to ES9-17 exposure).

Western-Blot

To verify that SAC fusion proteins were present in the plant cells, leaves from 1-month-old plants were vacuum infiltrated three times with 100 µM MG132 (inhibitor of proteasome). Treated leaves were grind in liquid nitrogen, and ground material resuspended in 4 ml of extraction buffer (100 mM Tris–HCl pH 7.5, 150 mM NaCl, 5 mM EDTA, 5% glycerol, 10 mM DTT, 0.5% Triton X-100, 1% Igepal and 1% protease inhibitors (Sigma) into ½ MS 100 µM MG132) and centrifuged at 17896 g for 40 min at 4°C to obtain the total protein extract in the supernatant. 1 ml of the total protein extract was incubated 20 min with 50 µL of magnetic protein G Dynabeads (Millipore) fused to a GFP monoclonal antibody (1/500 in PBS 0.002 % tween). Beads, antibodies and antibodies bund proteins were

magnetically precipitated on columns, eluted and denatured in 40 µL of Lamelli buffer 2X at 95°C for 5 min. 20 µL of immunoprecipitated proteins were loaded onto 7.5 % polyacrylamide gel, run for 105 min at 125 V and blotted on nitrocellulose membranes over-night at 20 V on ice. Membranes were blocked in 5 % milk dissolved in TBST buffer (10 mM Tris-HCL, 150 mM NaCL, 0.05 % Tween20) for 2 h at 4°C. mCIT tagged proteins were revealed by using respectively GFP monoclonal antibody (1/1000 in 5 % milk) as primary antibodies and anti-mousse IgG-HRP conjugated secondaries antibodies (1/5000 in TBST). Finally tagged proteins were detected by chemiluminescence using ECL, substrate to HRP enzyme, revelation.

Live cell imaging

Most images (see exceptions below) were acquired with the following spinning disk confocal microscope set up: inverted Zeiss microscope (AxioObserver Z1, Carl Zeiss Group, http://www.zeiss.com/) equipped with a spinning disk module (CSU-W1-T3, Yokogawa, www.yokogawa.com) and a ProEM+ 1024B camera (Princeton Instrument, http://www.princetoninstruments.com/) or Camera Prime 95B (www.photometrics.com) using a 63x Plan-Apochromat objective (numerical aperture 1.4, oil immersion). GFP and mCITRINE were excited with a 488 nm laser (150 mW) and fluorescence emission was filtered by a 525/50 nm BrightLine! single-band bandpass filter (Semrock, http://www.semrock.com/), mCHERRY en TdTOM was excited with a 561 nm laser (80 mW) and fluorescence emission was filtered by a 609/54 nm BrightLine! single-band bandpass filter (Semrock, http://www.semrock.com/). For quantitative imaging, pictures of epidermal root meristem cells were taken with detector settings optimized for low background and no pixel saturation. Care was taken to use similar confocal settings when comparing fluorescence intensity or for quantification.

Colocalization experiments were performed on an inverted Zeiss CLSM710 confocal microscope or an inverted Zeiss CLSM800 confocal microscope using a 63x Plan-apochromatic objective. Dual-color images were acquired by sequential line switching, allowing the separation of channels by both excitation and emission. In the case of colocalization, we also controlled for a complete absence of channel crosstalk. GFP was excited with a 488 nm laser, mCIT was excited with a 515nm laser and mCH/tdTOM were excited with a 561 nm laser. Imaging was performed in the root epidermis in cells that are at the onset of elongation.

Yeast two-hybrid screen

The yeast two hybrid screen was performed by hybrigenics services (https://www.hybrigenics-services.com/contents/our-services/interaction-discovery/ultimate-y2h-2), using the ULTImate Y2H screen against their Universal Arabidopsis Normalized library obtained using oligo_dT. A codon optimized residue (aa 499-966) of SAC9

gttaataatcaggggggatataacgctccccttccaccgggatgggaaaaaagagctgatgccgtaactggaaaatcatattatatagatcacaata
caaagacaacaacatggagtcatccatgtcctgataaaccatggaagagacttgacatgaggtttgaggaatttaagagatcaactatcttatctcctg
tgtcagaacttgccgatctttttctgcaacaaggtgatatccatgcaaccctctatactggctcgaaagctatgcacagccaaattctcaacatcttcagt
gaagaatcaggagcatttaaacagttttctgcagcacagaaaaacatgaagattacactacagagaagatataaaaatgctatggttgatagttcacg
gcaaaaacagctcgagatgtttctgggaatgaggcttttcaagcatcttccatcaattcctgtccagcctttacatgtactttctcgaccatctggtttcttt
ctgaaacctgtacctaacatgtccgaaagttccaatgatgggtccagtctgctgagtatcaagaggaaggacataacttggctatgtccacaagctgc
agatattgttgaattatttatctatctcagtgagccttgccatgtatgtcaacttctactgaccatatcacacggtgcggatgatttgacatgtccatccact
gtggacgtgagaactggacgccacatagaggaccttaaattagttgttgagttagttcaactggattaccgattacctgtaattatgttttctggacagg
gtgcttcaataccacgctgtgcaaatggtacaaatcttctggtacccttaccagggccaattagttctgaggatatggctgttactggagctggtgcac
gtcttcatgaaaaagatacgtcaagtctttcactgctatatgattttgaagaactagaaggacagttggatttcttaacccgtgtagttgctgttacattttat
ccagctggtgctgttagaattcctatgactcttggtcagatagaagtccttggaatttctcttccatggaaaggaatgtttacttgtgaacgtactggagg
aagattagctgaacttgcaaggaaaccagatgaagatggaagtccttttttcatcttgttctgacttgaatccgtttgctgcaacaacatctttacaggctg
aaactgtttccacaccagtacaacagaaggatccctttcccagtaatctgcttgacctttgacaggagaggactcttcttctgacccccttcccacaacc
agtggtggaatgtattgcaagtggaggcaatgacatgcttgatttcttagacgaagcagttgttgaatatcgcggctctgacactgttcctgacgggtc

t was cloned in a pB66 vector (N-GAL4-bait-C fusion). The screen was performed on 0.5 mM 3AT. 59 million interactions were analyzed, and 260 positive clones were sequenced (ATNOR_dT_hgx4515v1_pB66, Supplemental Table 2.

TIRF imaging

3 days old etiolated seedlings were used for hypocotyl epidermal cells observations. TIRF-VAEM imaging were made using an ilas2 TIRF microscope (Roper Scientific) with 100x Apo NA 1.46 Oil objective and a Prime 95B camera (Photometrics, https://www.photometrics.com/) and 1.5 coverslips were used (VWR 61-0136). Time lapses were acquired during 300 time-points for 300s (acquisition time 500ms). Spot density were measured using Spot_detector ImageJ macro (Bayle et al. 2017).
Particle identification and tracking was performed using ImageJ plugin Trackmate (https://research.pasteur.fr/fr/software/trackmate/) using following parameters: Particle min size 0.5, threshold 50, particles with contrast >0.04 were filtered. For tracks filtering 0 gap, min distance between two spots 0.2.

Dissociation indexes

Dissociation indexes of membrane lipid fluorescent biosensors were measured and calculated as previously described (Platre et al., 2018). Briefly, we calculated "indexNoDex", defined as the ratio between the fluorescence intensity (Mean Grey Value function of Fiji software) measured in two elliptical regions of interest (ROIs) from the plasma membrane region (one at the apical/basal plasma membrane region and one in the lateral PM region) and two elliptical ROIs in the cytosol in the mock condition.

Measures, counting and statistical analysis

Primary root length and number of lateral roots were manually measured from pictures. For comparing the primary root length and lateral root density between each genotype, we used a one-way ANOVA and post hoc Tukey HSD pairwise tests (95 % confidence level).

For quantitative imaging, pictures of epidermal root meristem cells were taken with detector settings optimized for low background and no pixel saturation. Care was taken to use similar confocal settings when comparing fluorescence intensity. Pseudo-colored images were obtained using the "Green Fire Blue" look-up-table (LUT) of Fiji software (http://www.fiji.sc/). The intracellular compartments ("spots") per cell were automatically counted.

We automatically measured the density of intracellular compartments labeled per root for each biosensor, and we used two-sided non-parametric Wilcoxon rank-sum tests to compare Col-0 and *sac9-3*$^{-/-}$ genotypes. To account for multiple testing, we used a Bonferroni correction and lowered the significance level of each test at alpha = 0.05/11 = 0.004.

Because the signal of mCIT-SAC9 is mainly soluble, no automatic spot detection could be used for colocalization analysis. Therefore, for comparing the number of intracellular compartments containing mCIT-SAC9 or mCIT-SAC9^{C459A} protein-fusions per cell across conditions, we manually counted them and used a generalized linear mixed-effect model (Poisson family) accounting for image ID (*id est* root) as a random factor was used. Since the localization of the marker for the membrane compartment was larger in z compared to the restricted localization of SAC9 (only present at the surface of the cell), we counted the number of mCIT-SAC9 labeled structure which was also labelled by the compartment markers. The same approach was used to deduce the localization of the mutated version of SAC9. We then computed a two-sided Tukey Post hoc tests (function "glht" in multicomp) to specifically compare each pair of conditions.

To assess the effect of the inhibitor PAO on anomalous mCIT-TUBBYc intracellular compartments, we manually counted their number per cell. We tested PAO effect and the effect of treatment duration

(30 min and 2 h) on the number of marked intracellular compartments using a generalized linear mixed-effect model (Poisson family) to account for image ID as a random factor. Two sided Post-hoc tests were performed using the package *lsmeans*. We compared the number of FM4-64 positive compartments in Col-0 and *sac9-3*$^{-/-}$ using a generalized linear mixed model (Poisson family) to account for image ID (*id est* root) as a random factor. The density of FM4-64 labeled compartments was also compared in Col-0 and *sac9-3*$^{-/-}$ using a linear mixed model accounting for image ID as a random factor; Type II Wald χ^2.

To compare the effects of BFA on FM4-64 treated Col-0 and *sac9-3*$^{-/-}$, we only compared the BFA treated Col-0 and *sac9-3*$^{-/-}$ seedlings using a generalized linear mixed model (Poisson family) with image ID (*id est* root) as a random factor (Type II Wald χ^2 test : $\chi^2 = 33.8$, $p < 0.001$).

To compare the effects of BFA on Col-0 and *sac9-3*$^{-/-}$ seedings expressing PIN2-GFP, we only compared the treatments BFA-Col-0 with BFA-Sac9 using a generalized linear mixed model (Poisson family) with image ID (*id est* root) as a random factor. (Type II Wald χ^2 test : $\chi^2 = 42.1$, $p < 0.001$). For dissociation index we performed all our statistical analyses in R (v. 3.6.1, (R Core Team, 2019), using R studio interface and the packages ggplot2 (Wickham 2016), lme4 (Bates et al. 2014), car (Fox and Weisberg 2011), multcomp (Hothorn et al. 2008) and lsmeans (Lenth and Lenth 2018). To compared TPLATE-GFP density between Col-0 and sac9-3$^{-/-}$ we used a two-sided non-parametric Kruskal Wallis rank-sum tests for each replicate and obtained each time a statistical difference (p.value < 0,05 between the two genotypes). Graphs were obtained with R and R-studio software, and customized with Inkscape (https://inkscape.org).

ACKNOWLEDGEMENTS

We are grateful to the SiCE group (RDP, Lyon, France), Dr Yohann Boutté (LBM, Bordeaux, France), Dr Fabrice Besnard and Dr Nicolas Doll (RDP, Lyon, France), Hugo Ducuing (INMG, Lyon, France), Sébastien This (CIRI, Lyon, France) and Augustin Le Bouquin (IGFL, Lyon, France), Dr Sophie Piquerez (IPS2, Paris-Saclay, France) for comments and discussions. We thank Justin Berger, Patrice Bolland, and Alexis Lacroix from our plant facility, and Claire Lionnet from the imaging platform. We are also grateful to Dr Daniël van Damme (VIB, Ghent, Belgium) for sharing with us T-PLATE-GFP and for discussions. We would like to thanks Pr Dr Erika Isono (University of Konstanz, Konstanz, Germany) for sharing SH3P2-sGFP transgenic line with us. We are also grateful to E. Russinova (VIB, Ghent, Belgium) for kindly providing us ES9-17; S. Bednarek for sharing markers and for discussions. This work was supported by two Seed Fund ENS LYON-2016 and LYON-2019 (to MCC), a Junior Investigator grant ANR-16-CE13-0021 (to MCC), ERC no. 3363360-APPL under FP/2007–2013 (to YJ). MD and AL were funded by Ph.D. fellowships from the French Ministry of Research and Higher Education.

FIGURES

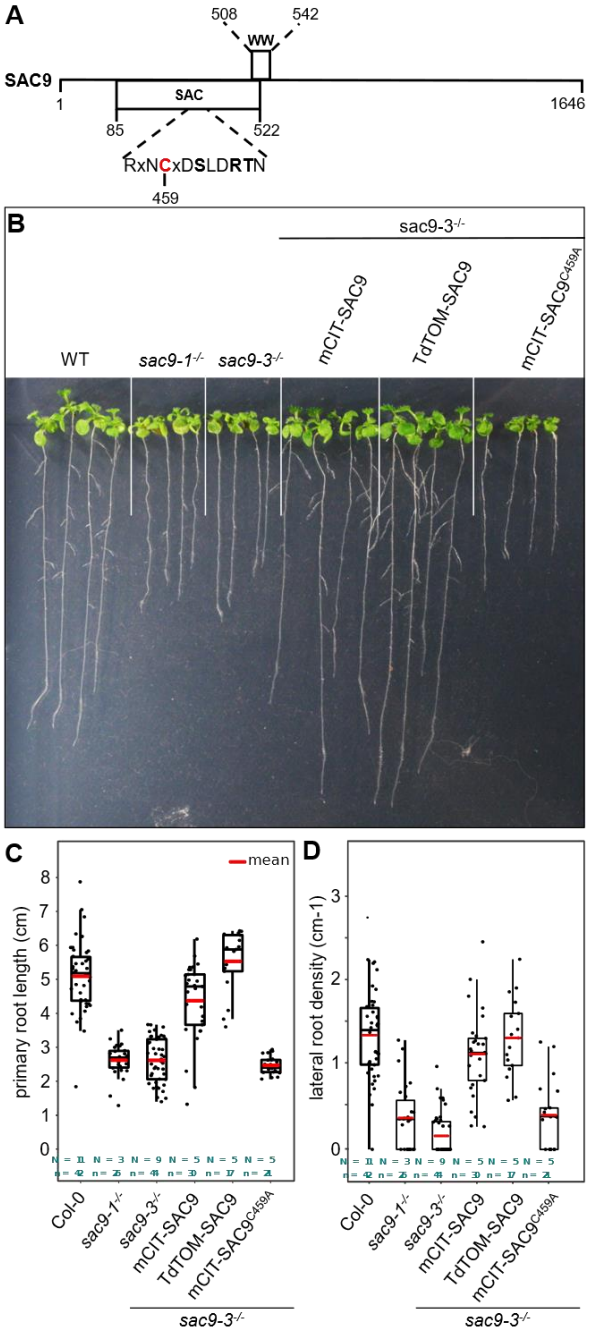

Figure 1. Structure-function analysis of SAC9. A, Schematic representation of SAC9 protein. The SAC catalytic domain, as well as the WW domain, are represented. **B,** Representative images of the macroscopic phenotype observed in (i) wild-type (Col-0), (ii) *sac9-1*$^{-/-}$ and *sac9-3*$^{-/-}$ loss of function mutants, (iii) *sac9-3*$^{-/-}$ complemented lines expressing full-length genomic DNA encoding SAC9 fused to fluorescent protein (mCIT-SAC9 and TdTOM-SAC9) or a mutated version of the catalytic cysteine residue within the C-x(5)-R-[TS] catalytic motif in the SAC domain (mCIT-SAC9^{C459A}; right panel). Pictures are taken 12 days post germination (dpg). **C,** Quantification of primary root length in *sac9-3*$^{-/-}$ homozygous mutants expressing mCIT-SAC9 and TdTOM-SAC9, mCIT-SAC9^{C459A} under the control of the native promoter (*SAC9prom*). Wild-type (Col-0) seedlings and two independent mutant alleles of *SAC9, sac9-1*$^{-/-}$ and *sac9-3*$^{-/-}$, are used as controls. **D,** Same as (C) but for the quantification of the lateral root density (ratio of the number of lateral roots to primary root length). In the plots, middle horizontal bars represent the median, while the bottom and top of each box represent the 25th and 75th percentiles, respectively. At most, the whiskers extend to 1.5 times the interquartile range, excluding data beyond. For range of value under 1,5 IQR, whiskers represent the range of maximum and minimum values. Details for statistical analysis can be found in the Methods section and supplementary Tables.

626

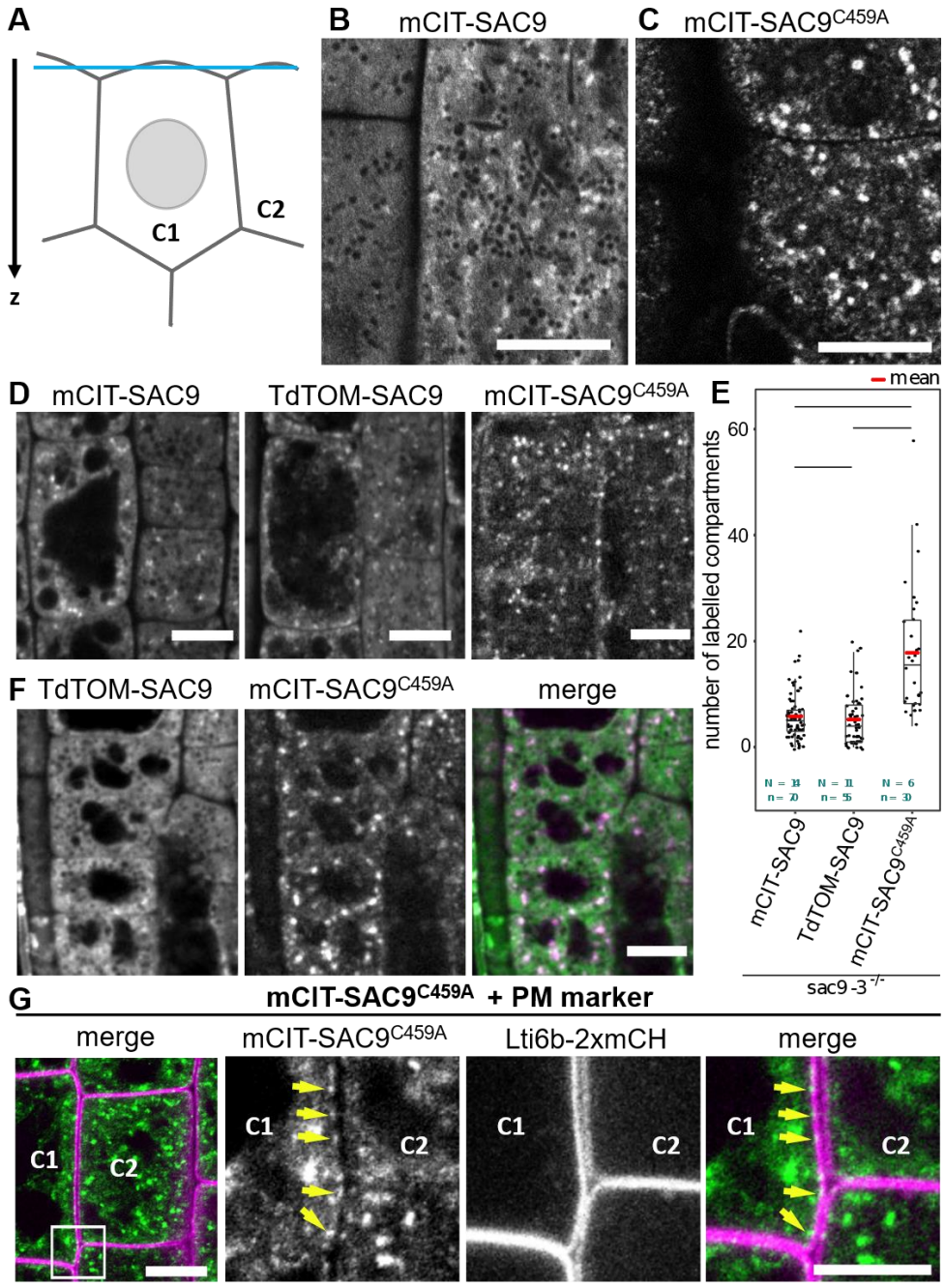

627

628 **Figure 2. A,** Schematic representation of two root epidermal cells (C1 and C2) imaged in this study. The blue bar represents the
629 depth at which the imaging was performed. **B,** Confocal images of the subcortical part Arabidopsis root epidermal cell expressing
630 mCIT-SAC9 under the control of *SAC9* native promoter (*SAC9prom*). **C,** Confocal images of the subcortical part Arabidopsis root
631 epidermal cell expressing mCIT-SAC9^{C459A} under the control of *SAC9* native promoter (*SAC9prom*). **D,** Representative images of
632 the fluorescent signal observe in sac9-3$^{-/-}$ mutant expressing mCIT-SAC9, TdTOM-SAC9 and mCIT-SAC9^{C459A}. **E,** Comparison
633 of the number of labeled intracellular compartments per cell in *sac9-3*$^{-/-}$ root epidermis expressing mCIT-SAC9 and TdTOM-SAC9,
634 mCIT-SAC9^{C459A}. In the plot, middle horizontal bars represent the median, while the bottom and top of each box represent the
635 25th and 75th percentiles, respectively. At most, the whiskers extend to 1.5 times the interquartile range, excluding data beyond.
636 For range of value under 1,5 IQR, whiskers represent the range of maximum and minimum values. **F,** Colocalization analysis on
637 *Ub10pro:TdTOM-SAC9* (magenta) and *SAC9pro:CIT-SAC9*^{C459A} (green). **G,** Co-visualization of *SAC9pro:CIT-SAC9*^{C459A} (green)
638 together with the membrane localized reporter Lti6b-2xmCH (magenta) close to the basal plasma membrane of an epidermal root
639 cell (C1). The yellow arrows indicate the intracellular compartment decorated by CIT-SAC9^{C459A} observed at the close vicinity to
640 the labelled plasma membrane. Scale bar: 10 µm in A-F; 5 µm in G (left panel) and 2 µm in the close up of G (right panel).

641

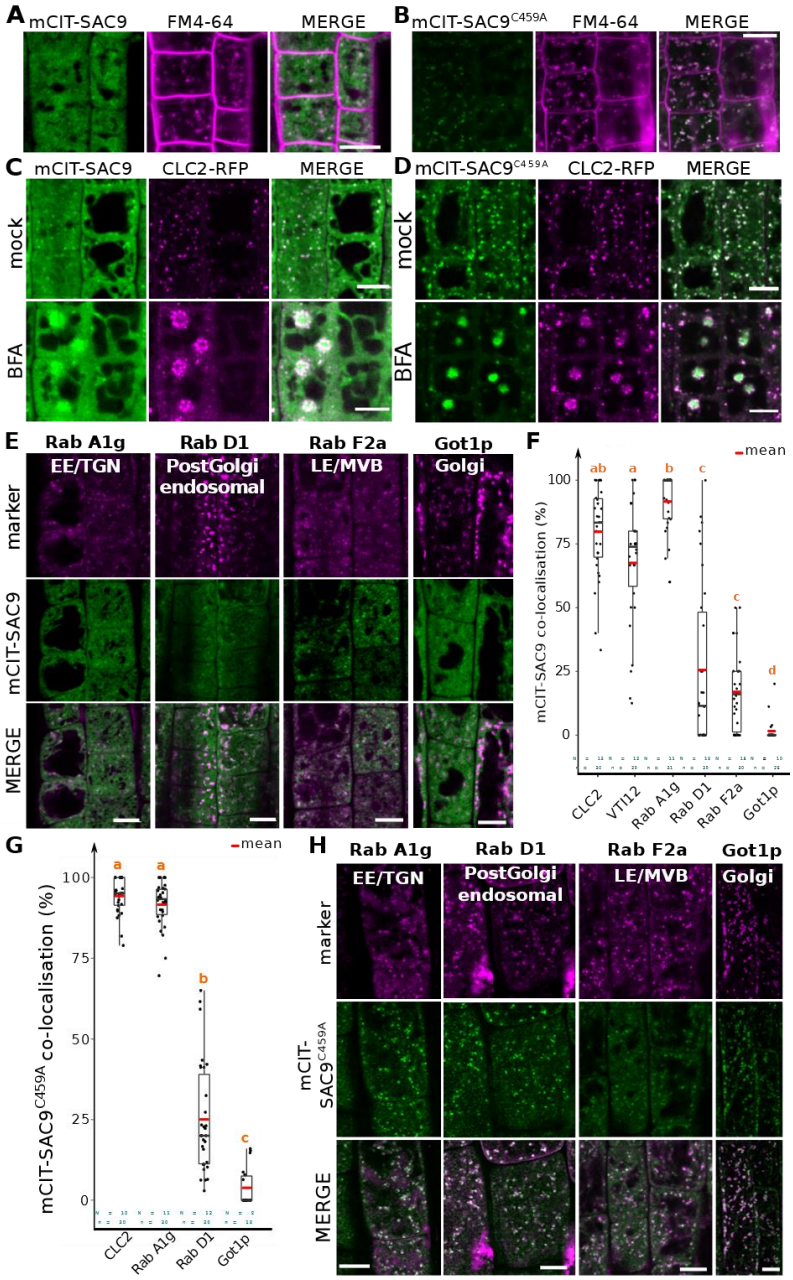

Figure 3. A, B Confocal images of *SAC9pro:mCIT-SAC9* (A, green) or *SAC9pro:mCIT- SAC9^{C459A}* (B, green) in vivo in Arabidopsis root epidermis together with the endocytic tracer FM4-64 (magenta). Scale bar: 10 µm. **C, D** Confocal images of Arabidopsis root epidermis co-expressing *SAC9pro:mCIT-SAC9* (C, green) or *SAC9pro:mCIT- SAC9^{C459A}* (D, green) together with and Clathrin Light Chain 2 (CLC2) fused to RFP (*UBQ10pro:CLC2-RFP*; magenta). Upper panel: fluorescent signals observed in the mock treatment; Lower panel: fluorescent signals observed after 50 µM 60 min BFA treatment. Scale bars: 10 µm. **E,** Confocal images of Arabidopsis root epidermis co-expressing *SAC9pro:mCIT-SAC9* (green) and TGN markers *mCH-RabA1g*, *mCH-RabD1* (magenta), the late endosome/pre--vacuolar compartment (LE/MVB) marker *mCH-RabF2a/Rha1* (magenta) and the Golgi marker *mCH-Got1p* (magenta). Scale bars: 10 µm. **F,** Quantification of the percentage of colocalization between mCIT-SAC9 and a given endosomal compartment marker per cell. **G,** Quantification of the percentage of colocalization between mCIT-SAC9^{C459A} and a given endosomal compartment marker. Similar letters correspond to markers with non-significantly different percentages of colocalization with mCIT-SAC9^{C459A} (one-way ANOVA and post hoc Tuckey HSD pairwise test with a 95 % confidence level). In the plots, middle horizontal bars represent the median, while the bottom and top of each box represent the 25th and 75th percentiles, respectively. At most, the whiskers extend to 1.5 times the interquartile range, excluding data beyond. For range of value under 1,5 IQR, whiskers represent the range of maximum and minimum values. **E,** Confocal images of Arabidopsis root epidermis co-expressing *SAC9pro:mCIT-SAC9^{C459A}* (green) and TGN markers *mCH-RabA1g*, *mCH-RabD1* (magenta), the late endosome/pre-vacuolar compartment (LE/MVB) marker *mCH-RabF2a/Rha1* (magenta) and the Golgi marker *mCH-Got1p* (magenta). Scale bars: 10 µm.

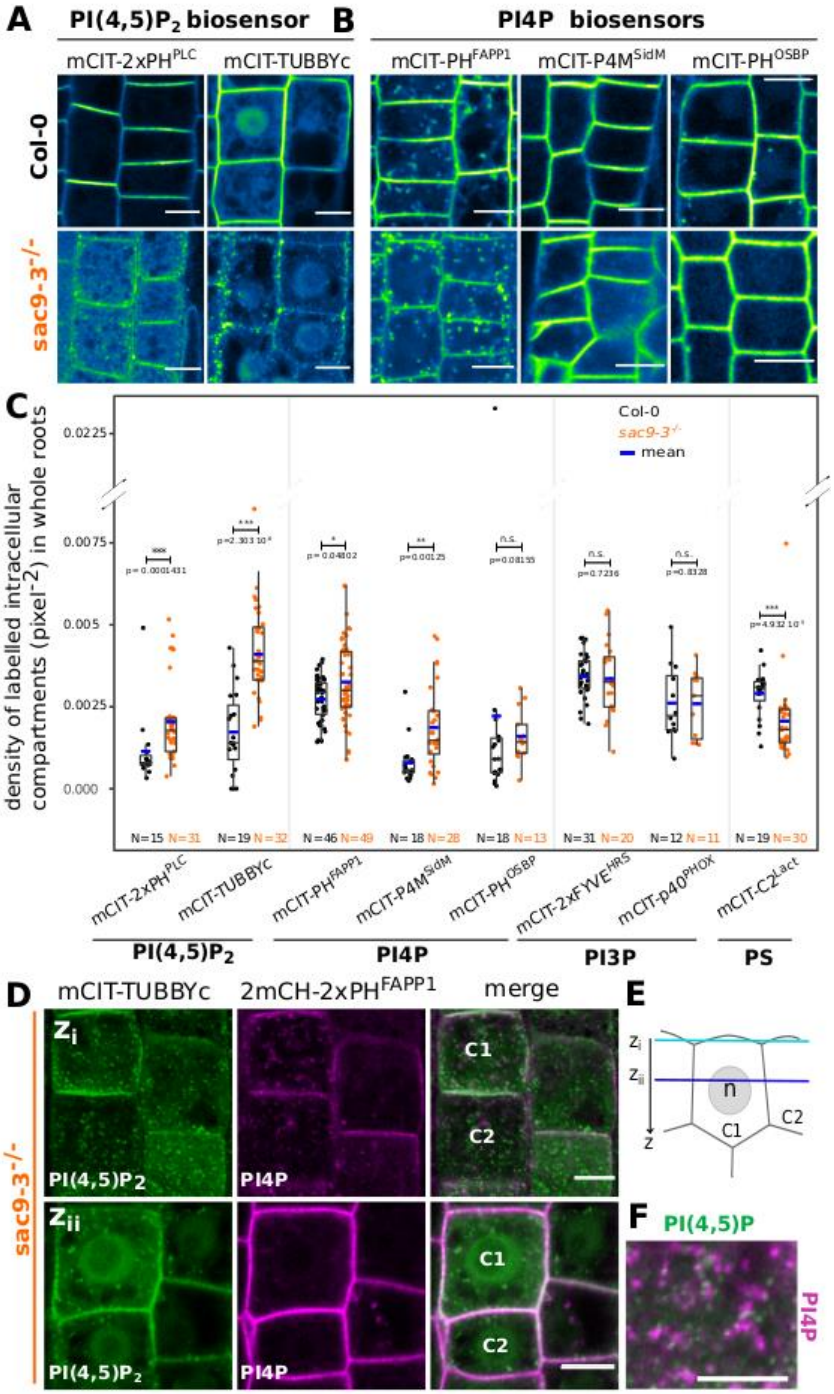

Figure 4. A, Confocal images of Arabidopsis root epidermis expressing mCIT-tagged $PI(4,5)P_2$ sensors in WT (Col-0) and *sac9-3*$^{-/-}$ genetic backgrounds. **B,** Confocal images of Arabidopsis root epidermis expressing mCIT-tagged PI4P sensors in Wild-type (Col-0) and *sac9-3*$^{-/-}$ genetic backgrounds. Fluorescence intensity is color-coded (green fire blue scale). **C,** Quantification of density of labelled intracellular compartments (pixel^{-2}) in whole roots epidermis expressing mCIT-tagged lipid sensors in wild-type (Col-0) and *sac9-3*$^{-/-}$. Non-parametric Wilcoxon rank sum tests with Bonferroni correction. In the plots, middle horizontal bars represent the median, while the bottom and top of each box represent the 25th and 75th percentiles, respectively. At most, the whiskers extend to 1.5 times the interquartile range, excluding data beyond. For range of value under 1,5 IQR, whiskers represent the range of maximum and minimum values. Details for statistical analysis can be found in the Methods section and supplementary Tables. **D,** Confocal images of *sac9-3*$^{-/-}$ Arabidopsis root epidermal cell (C1 and C2) expressing *mCIT-TUBBYc* (green) and *2xmCH-PH*^{FAPP1} (magenta) at their cortex (upper panel, Zi) and at their center (bottom panel, Zii). **E,** Schematic representation of two root epidermal cells (C1 and C2) imaged in D. The blue bars represent the depth at which the imaging was performed. **F,** close up (form a different cell) of the distribution of the intracellular compartments in *sac9-3*$^{-/-}$ epidermal cell labelled by mCIT-TUBBYc (green) and 2xmCH-PH^{FAPP1} (magenta). Scale bar: 10 µm in A-D, 5 µm in F.

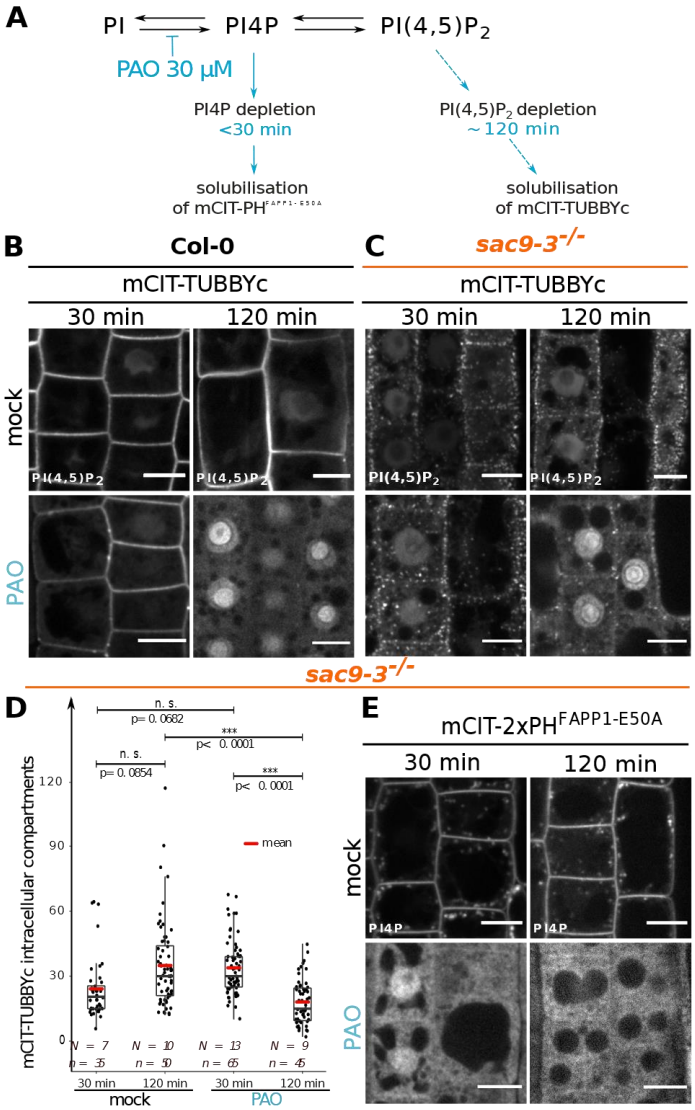

Figure 5. A, Schematic representation of the mode of action of the PAO on the PI4P and PI(4,5)P_2 metabolism based on previously published work (Doumane et al. 2020; Platre et al. 2018). **B,** Confocal images of WT root epidermal cells expressing mCIT-TUBBYc PI(4,5)P_2 biosensor that underwent mock, or 30 µM PAO treatments for 30- or 120- min. **C,** Confocal images of *sac9-3*$^{-/-}$ root epidermal cells expressing mCIT-TUBBYc PI(4,5)P_2 biosensor that underwent mock, or 30 µM PAO treatments for 30- or 120- min. **D,** Quantification of the number of mCIT-TUBBYc labeled intracellular compartments per cell in *sac9-3*$^{-/-}$ following mock, or 30 µM PAO treatments for 30- or 120- min. Generalized linear mixed effect model (Poisson family) to account for root as a random factor, and two sided post hoc *lsmeans* pair wise test with a 95 % confidence level. In the plot, middle horizontal bars represent the median, while the bottom and top of each box represent the 25th and 75th percentiles, respectively. At most, the whiskers extend to 1.5 times the interquartile range, excluding data beyond. For range of value under 1,5 IQR, whiskers represent the range of maximum and minimum values. All statistical tests were two-sided. **E,** Confocal images of *sac9-3*$^{-/-}$ root epidermal cells expressing mCIT-PH$^{FAPP1-E50A}$ PI4P biosensor that underwent mock or 30 µM PAO treatments for 30- or 120- min. Scale bar: 10 µm.

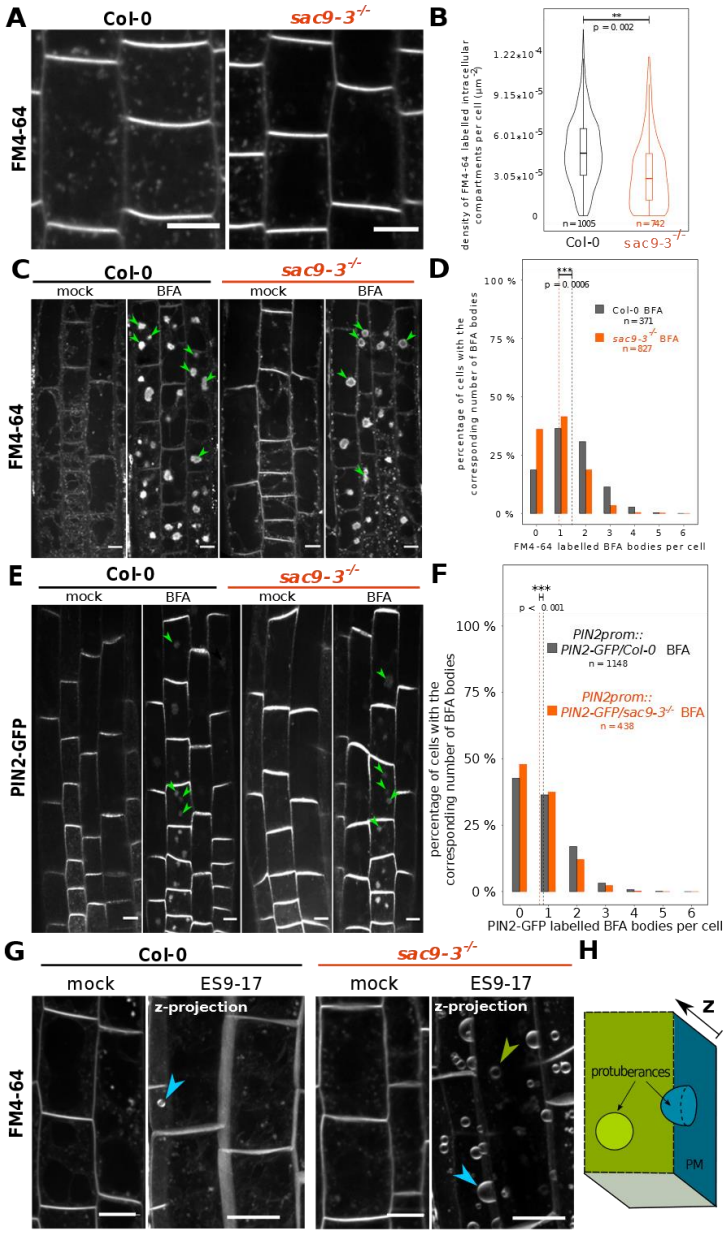

688

689 **Figure 6. A,** Representative images of Col-0 and *sac9-3*$^{-/-}$ seedlings treated for 30 min with FM4-64, which is endocytosed and
690 labels endocytic intracellular compartments. Scale bar: 10 µm. **B,** Quantification from the experiment showed in (A). Violin and
691 box plots quantifying the number of FM4-64 labeled intracellular compartments in Col-0 and *sac9-3*$^{-/-}$. **C,** Representative images of
692 root epidermis following BFA and FM4-64 treatment of Col-0 and *sac9-3*$^{-/-}$ seedlings. Examples of FM4-64 labeled BFA bodies are
693 pointed out (green arrowheads). **D,** Quantification from the experiment showed in (C). For Col-0 and *sac9-3*$^{-/-}$, the proportion (%)
694 of cells containing from none to six BFA bodies is displayed. Dotted line: means. **E,** Representative images following BFA
695 treatment of PIN2-GFP/WT and PIN2-GFP/*sac9-3*$^{-/-}$ seedlings. Examples of PIN2-GFP labeled BFA bodies are pointed out
696 (green arrowheads). Scale bars: 10 µm. **F,** Quantification from the experiment showed in (E). For *PIN2-GFP*/WT and PIN2-
697 GFP/*sac9-3*$^{-/-}$, the proportion (%) of cells containing from none to six BFA bodies is displayed. Dotted line: means. **G,** Over-
698 sensitivity of *sac9-3*$^{-/-}$ to prolonged inhibition of endocytosis. Seedlings were treated 180 min with 30 µM ES9-17 or DMSO (mock),
699 FM4-64 being added after 30 min (150 min of exposure). The picture showed after the ES9-17 treatment are the results of the
700 projection of a z-stack. **H,** ES9-17 treatments led to dome-shaped plasma membrane invagination. blue arrowheads: invaginations
701 with an obvious connection to the plasma membrane; green arrowheads: invaginations without a clear connection to the plasma
702 membrane (often connected to medullar plasma membrane). Scale bars: 10 µm.

703

704

705

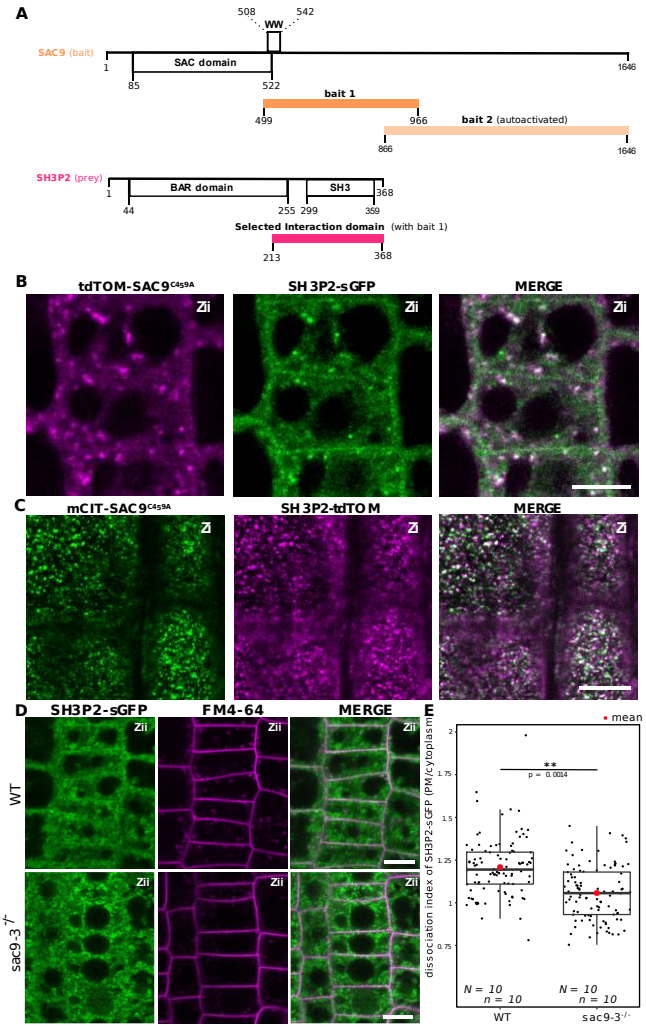

Figure 7. A, Schematic representation of the yeast two-hybrid screen using SAC9 as a bait, where SH3P2 was found as a protein partner. The selected interaction domain (interacting with bait 1) corresponds to the amino acid sequence shared by all the eleven prey fragments matching the same reference protein. Note that one other fragment of SAC9 was attended to be screened for interacting proteins (bait 2), but the construct was autoactivate in yeast. For design purpose, the scale between SAC9 and SH3P2 was not respected. **B,** Representatives images of the in vivo colocalization analysis between tdTOM-SAC9^{C459A} (magenta) and SH3P2-sGFP (green) in a distal region from the plasma membrane. Scale =5µm. **C,** Representatives images of the in vivo colocalization analysis between mCIT-SAC9^{C459A} (green) and SH3P2-tdTOM (magenta) near the plasma membrane. Scale =5µm. The light blue line (zi) corresponds to the in vivo imaging near the plasma membrane observed by confocal imaging and the dark blue line (zii) corresponds to the in vivo imaging in a distal region from the plasma membrane. (See Figure 4E for details) **D,** Representatives images of the SH3P2-sGFP localization (green) in WT and *sac9-3* mutant in which the plasma membrane was labelled using FM4-64 (magenta). **E,** Double blinded quantification of the dissociation index of SH3P2-sGFP in WT and *sac9-3* mutant in which the plasma membrane was labelled using FM4-64. Linear mixed model (lmer in lme4) then type II Wald chisquare test: Chisq = 10.152, df=1, p = 0.001441. In the plot, middle horizontal bars represent the median, while the bottom and top of each box represent the 25th and 75th percentiles, respectively. At most, the whiskers extend to 1.5 times the interquartile range, excluding data beyond. For range of value under 1,5 IQR, whiskers represent the range of maximum and minimum values.

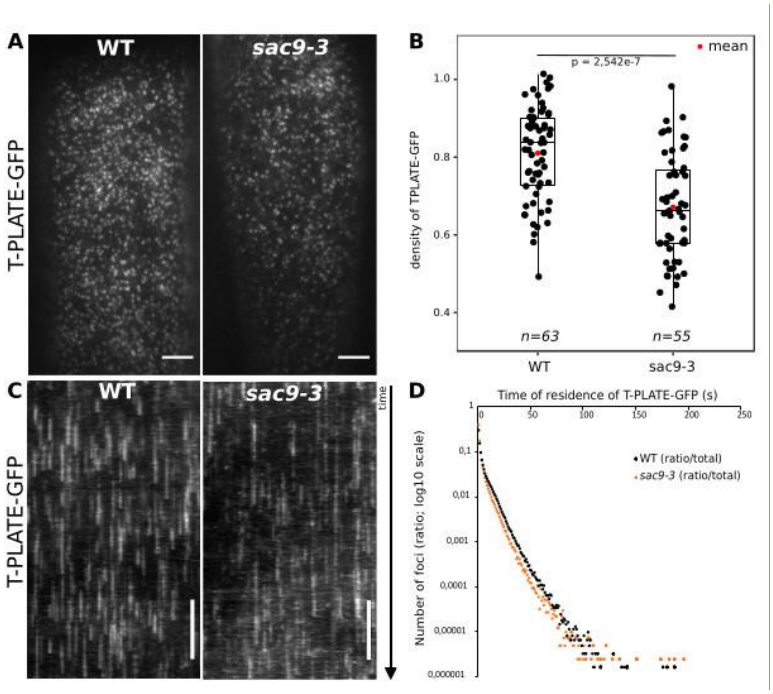

Figure 8. A, Representatives images of the TPLATE-GFP localization in WT and *sac9-3* mutant at the plasma membrane observed by TIRF microscopy in etiolated hypocotyl. Scale = 5µm. **B,** Quantification of the density at the plasma membrane of SH3P2-sGFP in WT and *sac9-3* mutant observed by TIRF microscopy. Only one of the three replicates is represented. In the plots, middle horizontal bars represent the median, while the bottom and top of each box represent the 25th and 75th percentiles, respectively. At most, the whiskers extend to 1.5 times the interquartile range, excluding data beyond. For range of value under 1,5 IQR, whiskers represent the range of maximum and minimum values. **C,** Representatives kymograph of the TPLATE-GFP dynamics at the plasma membrane in WT and *sac9-3* mutant observed by TIRF microscopy in etiolated hypocotyl over 5 min, scale =60s. D, Quantification of the time of residency at the plasma membrane of TPLATE-GFP in WT (black dots) and *sac9-3* mutant (oranges dots) observed by TIRF microscopy in a time lapses acquired during 300 time-points for 300s (acquisition time 500ms). The data are represented in a log10 scale for the residency time at the PM, and the time scale is represented in sec.

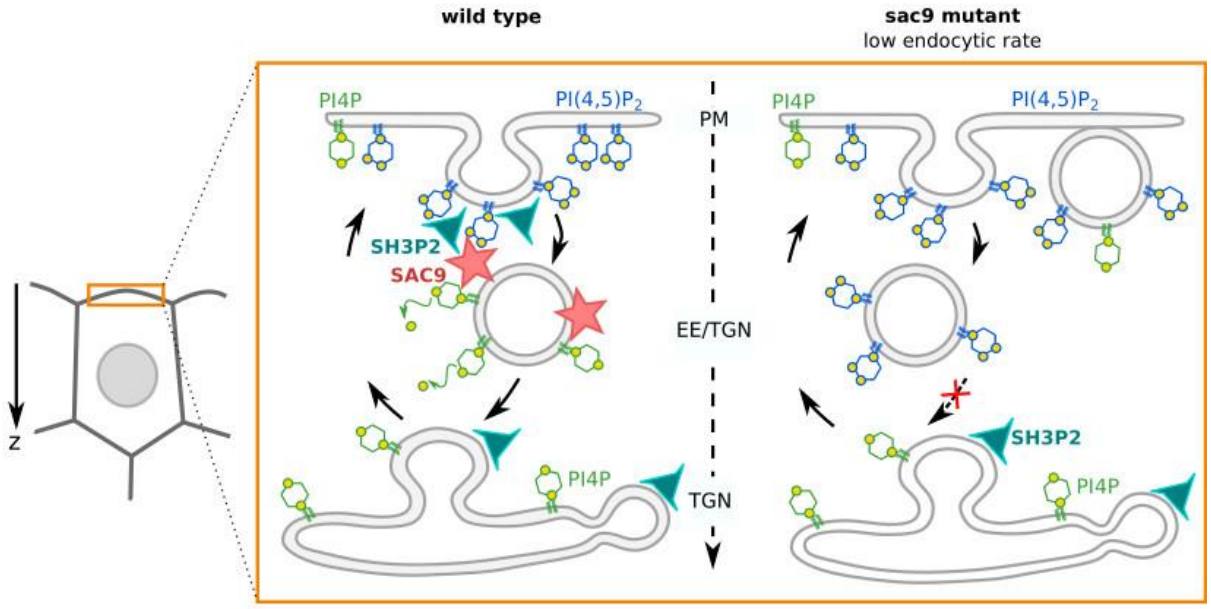

Figure 9. Model for the mode of action of SAC9 in regulating the $PI(4,5)P_2$ homeostasis at the close vicinity with the plasma membrane. In wild type plants, SAC9 restricts the localization of $PI(4,5)P_2$ at the plasma membrane allowing endocytic processes to occur. In the absence of SAC9, endocytosis $PI(4,5)P_2$ accumulates in atypical endomembrane compartments that are no longer able to fuse with the TGN because of their abnormal anionic lipid signature. SAC9 interacts with SH3P2 close to the plasma membrane. The defects in $PI(4,5)P_2$ patterning in absence of SAC9 leads to decreasing of the endocytic rate and the formation of membrane protuberances in contact with the plasma membrane.

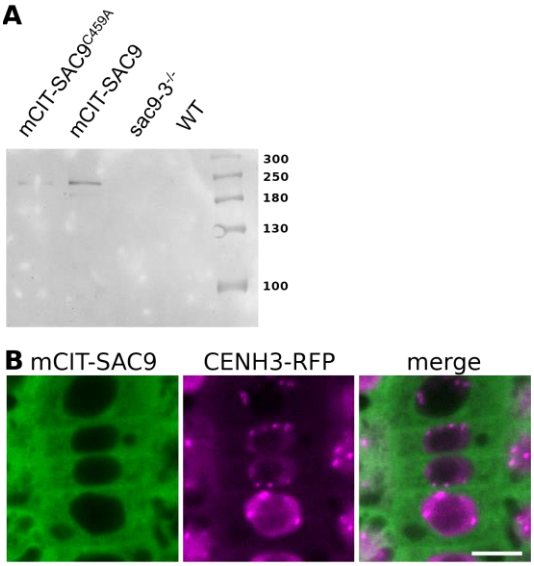

Supplemental Fig.1. A, Western blot analysis. Leaf lysates from Col-0, *sac9-3*$^{+/-}$, *SAC9pro:mCIT-SAC9*/*sac9-3*$^{+/-}$, *SAC9pro:mCIT-SAC9*^{C459A}/*sac9-3*$^{+/-}$ were immunoprecipitated with an anti-GFP antibody, run on an SDS-PAGE and immunoblotted with anti-GFP primary antibody. **B,** Confocal imaging of mCIT-SAC9 (green) together with the nuclear marker CENH3-RFP (magenta). Scale bars: 10 μm.

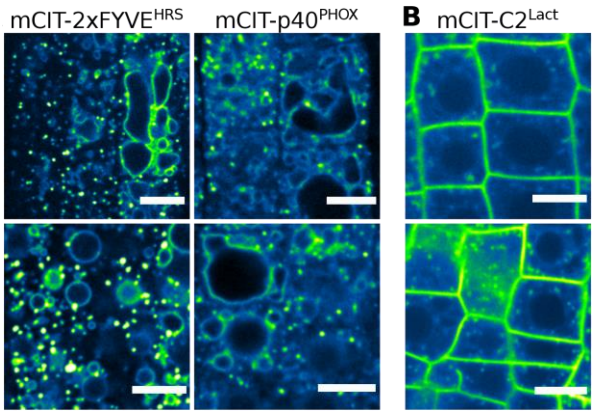

Supplemental Fig.2. A, Representative confocal images of *Arabidopsis* root epidermis expressing mCIT-tagged lipid sensors for PI3P in wild-type (Col-0) and *sac9-3*$^{+/-}$ genetic backgrounds. **B,** Confocal images of Arabidopsis root epidermis expressing mCIT-tagged lipid sensors for phosphatidylserine (PS) in wild-type (Col-0) and *sac9-3*$^{+/-}$ genetic backgrounds. Fluorescence intensity is color-coded (green fire blue scale). Scale bars: 10 μm.

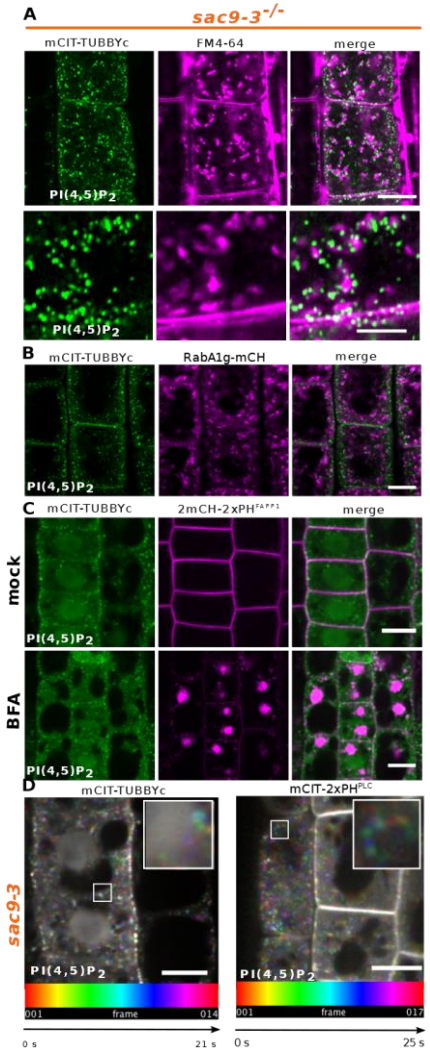

Supplemental Fig.3. A, Confocal images of *sac9-3*$^{-/-}$ Arabidopsis root epidermis expressing mCIT-TUBBYc (green) and *in vivo* stained with FM4-64 endocytic tracer (magenta). **B,** Confocal images of *sac9-3*$^{-/-}$ root epidermal cells co-expressing mCIT-TUBBYc (green) and the TGN marker RabA1g-mCH (magenta). **C,** Confocal images of *sac9-3*$^{-/-}$ root epidermal cells co-expressing mCIT-TUBBYc (green) and 2xmCH-PH^{FAPP1} (magenta). Upper panel: fluorescent signals observed in the mock treatment; lower panel: fluorescent signal observed after 50 µM 60 min BFA treatment. **D,** Temporal-color coded XY 2D image of mCIT-2xPH^{PLC} and mCIT-TUBBYc in *sac9-3*$^{-/-}$ root epidermis (Fiji Spectrum Temporal-color code). Scale bar: 10 µm.

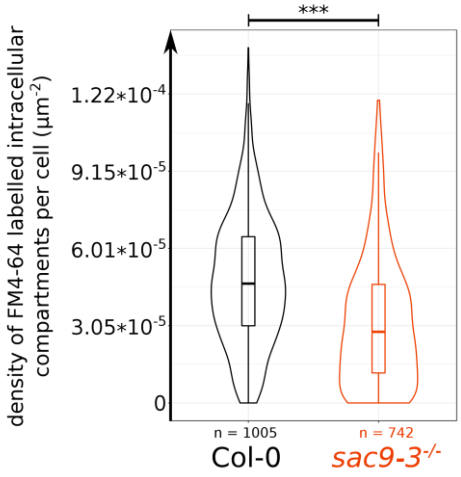

764

765 **Supplemental Fig.4.** Quantification from the FM4-64 uptake assay. Violin and box plots quantifying the density of FM4-64
766 labeled intracellular compartments in Col-0 and *sac9-3*$^{-/-}$. N: number of cells. Linear mixed model (Poisson family) to account for
767 root as a random factor. *** p-value < 0.0005.

768

769 **Supplemental Movie 1.** Time-lapse imaging of mCIT-SAC9 using spinning disk confocal microscope

770 **Supplemental Movie 2.** Time-lapse imaging of mCIT-2xPH^{PLC} in sac9 mutant (1 sec per frame) using spinning disk confocal
771 microscope.

772 **Supplemental Movie 3.** Time-lapse imaging of T-PLATE-GFP at the plasma membrane of WT and in sac9-3 mutant using TIRF
773 microscopy. Time lapses were acquired during 300 time-points for 300s (acquisition time 500ms).

REFERENCES

Abad U, Sassi M, Traas J (2017) Flower development: from morphodynamics to morphomechanics. Philosophical transactions of the Royal Society of London Series B, Biological sciences 372 (1720). doi:10.1098/rstb.2015.0545

Adamowski M, Narasimhan M, Kania U, Glanc M, De Jaeger G, Friml J (2018) A Functional Study of AUXILIN-LIKE1 and 2, Two Putative Clathrin Uncoating Factors in Arabidopsis. The Plant cell 30 (3):700-716. doi:10.1105/tpc.17.00785

Ahn G, Kim H, Kim DH, Hanh H, Yoon Y, Singaram I, Wijesinghe KJ, Johnson KA, Zhuang X, Liang Z, Stahelin RV, Jiang L, Cho W, Kang BH, Hwang I (2017) SH3 Domain-Containing Protein 2 Plays a Crucial Role at the Step of Membrane Tubulation during Cell Plate Formation. The Plant cell 29 (6):1388-1405. doi:10.1105/tpc.17.00108

Armengot L, Marquès-Bueno MM, Jaillais Y (2016) Regulation of polar auxin transport by protein and lipid kinases. Journal of experimental botany 67 (14):4015-4037

Balla T (2013) Phosphoinositides: tiny lipids with giant impact on cell regulation. Physiol Rev 93 (3):1019-1137. doi:10.1152/physrev.00028.2012

Bates D, Mächler M, Bolker B, Walker S (2014) Fitting linear mixed-effects models using lme4. arXiv preprint arXiv:14065823

Ben El Kadhi K, Roubinet C, Solinet S, Emery G, Carreno S (2011) The inositol 5-phosphatase dOCRL controls PI(4,5)P2 homeostasis and is necessary for cytokinesis. Current biology : CB 21 (12):1074-1079. doi:10.1016/j.cub.2011.05.030

Carim SC, Ben El Kadhi K, Yan G, Sweeney ST, Hickson GR, Carreno S, Lowe M (2019) IPIP27 Coordinates PtdIns(4,5)P2 Homeostasis for Successful Cytokinesis. Current biology : CB 29 (5):775-789 e777. doi:10.1016/j.cub.2019.01.043

Carland F, Nelson T (2009) CVP2- and CVL1-mediated phosphoinositide signaling as a regulator of the ARF GAP SFC/VAN3 in establishment of foliar vein patterns. The Plant journal : for cell and molecular biology 59 (6):895-907. doi:10.1111/j.1365-313X.2009.03920.x

Carland FM, Nelson T (2004) Cotyledon vascular pattern2-mediated inositol (1,4,5) triphosphate signal transduction is essential for closed venation patterns of Arabidopsis foliar organs. The Plant cell 16 (5):1263-1275. doi:10.1105/tpc.021030

Cauvin C, Rosendale M, Gupta-Rossi N, Rocancourt M, Larraufie P, Salomon R, Perrais D, Echard A (2016) Rab35 GTPase Triggers Switch-like Recruitment of the Lowe Syndrome Lipid Phosphatase OCRL on Newborn Endosomes. Current biology : CB 26 (1):120-128. doi:10.1016/j.cub.2015.11.040

De Matteis MA, Staiano L, Emma F, Devuyst O (2017) The 5-phosphatase OCRL in Lowe syndrome and Dent disease 2. Nature Reviews Nephrology 13 (8):455-470. doi:10.1038/nrneph.2017.83

Dejonghe W, Sharma I, Denoo B, De Munck S, Lu Q, Mishev K, Bulut H, Mylle E, De Rycke R, Vasileva M, Savatin DV, Nerinckx W, Staes A, Drozdzecki A, Audenaert D, Yperman K, Madder A, Friml J, Van Damme D, Gevaert K, Haucke V, Savvides SN, Winne J, Russinova E (2019) Disruption of endocytosis through chemical inhibition of clathrin heavy chain function. Nat Chem Biol 15 (6):641-649. doi:10.1038/s41589-019-0262-1

Del Signore SJ, Biber SA, Lehmann KS, Heimler SR, Rosenfeld BH, Eskin TL, Sweeney ST, Rodal AA (2017) dOCRL maintains immune cell quiescence by regulating endosomal traffic. PLoS Genet 13 (10):e1007052. doi:10.1371/journal.pgen.1007052

Dettmer J, Hong-Hermesdorf A, Stierhof YD, Schumacher K (2006) Vacuolar H+-ATPase activity is required for endocytic and secretory trafficking in Arabidopsis. The Plant cell 18 (3):715-730. doi:10.1105/tpc.105.037978

Doumane M, Colin L, Lebecq A, Fangain A, Bareille J, Hamant O, Belkhadir Y, Jaillais Y, Caillaud M-C (2020) iDePP: a genetically encoded system for the inducible depletion of PI (4, 5) P2 in Arabidopsis thaliana. bioRxiv

826 Doumane M, Lebecq A, Colin L, Fangain A, Stevens FD, Bareille J, Hamant O, Belkhadir Y,
827 Munnik T, Jaillais Y, Caillaud MC (2021) Inducible depletion of PI(4,5)P2 by the
828 synthetic iDePP system in Arabidopsis. Nat Plants 7 (5):587-597. doi:10.1038/s41477-
829 021-00907-z
830 Flanagan CA, Schnieders EA, Emerick AW, Kunisawa R, Admon A, Thorner J (1993)
831 Phosphatidylinositol 4-kinase: gene structure and requirement for yeast cell viability.
832 Science 262 (5138):1444-1448. doi:10.1126/science.8248783
833 Fox J, Weisberg S (2011) The car package contains functions and data sets associated with
834 the book an R companion to applied regression. R-Project.
835 Geldner N, Denervaud-Tendon V, Hyman DL, Mayer U, Stierhof YD, Chory J (2009) Rapid,
836 combinatorial analysis of membrane compartments in intact plants with a multicolor
837 marker set. The Plant journal : for cell and molecular biology 59 (1):169-178.
838 doi:10.1111/j.1365-313X.2009.03851.x
839 Golani Y, Kaye Y, Gilhar O, Ercetin M, Gillaspy G, Levine A (2013) Inositol polyphosphate
840 phosphatidylinositol 5-phosphatase9 (At5ptase9) controls plant salt tolerance by
841 regulating endocytosis. Molecular plant 6 (6):1781-1794. doi:10.1093/mp/sst072
842 Gujas B, Cruz TMD, Kastanaki E, Vermeer JEM, Munnik T, Rodriguez-Villalon A (2017)
843 Perturbing phosphoinositide homeostasis oppositely affects vascular differentiation in
844 Arabidopsis thaliana roots. Development 144 (19):3578-3589.
845 doi:10.1242/dev.155788
846 Guo S, Stolz LE, Lemrow SM, York JD (1999) SAC1-like domains of yeast SAC1, INP52, and
847 INP53 and of human synaptojanin encode polyphosphoinositide phosphatases. The
848 Journal of biological chemistry 274 (19):12990-12995
849 Gurung R, Tan A, Ooms LM, McGrath MJ, Huysmans RD, Munday AD, Prescott M, Whisstock
850 JC, Mitchell CA (2003) Identification of a novel domain in two mammalian inositol-
851 polyphosphate 5-phosphatases that mediates membrane ruffle localization. The
852 inositol 5-phosphatase skip localizes to the endoplasmic reticulum and translocates to
853 membrane ruffles following epidermal growth factor stimulation. The Journal of
854 biological chemistry 278 (13):11376-11385. doi:10.1074/jbc.M209991200
855 He K, Marsland Iii R, Upadhyayula S, Song E, Dang S, Capraro BR, Wang W, Skillern W,
856 Gaudin R, Ma M, Kirchhausen T (2017) Dynamics of phosphoinositide conversion in
857 clathrin-mediated endocytic traffic. Nature 552 (7685):410-414.
858 doi:10.1038/nature25146
859 Hothorn T, Bretz F, Westfall P, Heiberger RM (2008) Multcomp: simultaneous inference for
860 general linear hypotheses. R package version:1.0-3
861 Hughes WE, Woscholski R, Cooke FT, Patrick RS, Dove SK, McDonald NQ, Parker PJ (2000)
862 SAC1 encodes a regulated lipid phosphoinositide phosphatase, defects in which can
863 be suppressed by the homologous Inp52p and Inp53p phosphatases. The Journal of
864 biological chemistry 275 (2):801-808
865 Ischebeck T, Werner S, Krishnamoorthy P, Lerche J, Meijon M, Stenzel I, Lofke C, Wiessner
866 T, Im YJ, Perera IY, Iven T, Feussner I, Busch W, Boss WF, Teichmann T, Hause B,
867 Persson S, Heilmann I (2013) Phosphatidylinositol 4,5-bisphosphate influences PIN
868 polarization by controlling clathrin-mediated membrane trafficking in Arabidopsis. The
869 Plant cell 25 (12):4894-4911. doi:10.1105/tpc.113.116582
870 Karimi M, Depicker A, Hilson P (2007) Recombinational cloning with plant gateway vectors.
871 Plant physiology 145 (4):1144-1154. doi:10.1104/pp.107.106989
872 Lenth R, Lenth MR (2018) Package 'lsmeans'. The American Statistician 34 (4):216-221
873 Mei Y, Jia WJ, Chu YJ, Xue HW (2012) Arabidopsis phosphatidylinositol monophosphate 5-
874 kinase 2 is involved in root gravitropism through regulation of polar auxin transport by
875 affecting the cycling of PIN proteins. Cell research 22 (3):581-597.
876 doi:10.1038/cr.2011.150
877 Mochizuki Y, Takenawa T (1999) Novel inositol polyphosphate 5-phosphatase localizes at
878 membrane ruffles. The Journal of biological chemistry 274 (51):36790-36795.
879 doi:10.1074/jbc.274.51.36790

880 Nagel MK, Kalinowska K, Vogel K, Reynolds GD, Wu Z, Anzenberger F, Ichikawa M, Tsutsumi
881 C, Sato MH, Kuster B, Bednarek SY, Isono E (2017) Arabidopsis SH3P2 is an
882 ubiquitin-binding protein that functions together with ESCRT-I and the deubiquitylating
883 enzyme AMSH3. Proceedings of the National Academy of Sciences of the United
884 States of America 114 (34):E7197-E7204. doi:10.1073/pnas.1710866114
885 Nandez R, Balkin DM, Messa M, Liang L, Paradise S, Czapla H, Hein MY, Duncan JS, Mann
886 M, De Camilli P (2014) A role of OCRL in clathrin-coated pit dynamics and uncoating
887 revealed by studies of Lowe syndrome cells. Elife 3:e02975. doi:10.7554/eLife.02975
888 Narasimhan M, Johnson A, Prizak R, Kaufmann WA, Tan S, Casillas-Perez B, Friml J (2020)
889 Evolutionarily unique mechanistic framework of clathrin-mediated endocytosis in
890 plants. Elife 9. doi:10.7554/eLife.52067
891 Noack L, Bayle V, Armengot L, Rozier F, Mamode-Cassim A, Stevens F, Caillaud M, Munnik
892 T, Mongrand S, Jaillais Y (2020) A nanodomain anchored-scaffolding complex is
893 required for PI4Kα function and localization in plants.
894 bioRxiv:2020.2012.2008.415711. doi:10.1101/2020.12.08.415711
895 Noack LC, Jaillais Y (2017) Precision targeting by phosphoinositides: how PIs direct
896 endomembrane trafficking in plants. Current opinion in plant biology 40:22-33.
897 doi:10.1016/j.pbi.2017.06.017
898 Noack LC, Jaillais Y (2020) Functions of Anionic Lipids in Plants. Annual review of plant
899 biology 71:71-102. doi:10.1146/annurev-arplant-081519-035910
900 Novakova P, Hirsch S, Feraru E, Tejos R, van Wijk R, Viaene T, Heilmann M, Lerche J, De
901 Rycke R, Feraru MI, Grones P, Van Montagu M, Heilmann I, Munnik T, Friml J (2014)
902 SAC phosphoinositide phosphatases at the tonoplast mediate vacuolar function in
903 Arabidopsis. Proceedings of the National Academy of Sciences of the United States of
904 America 111 (7):2818-2823. doi:10.1073/pnas.1324264111
905 Paez Valencia J, Goodman K, Otegui MS (2016) Endocytosis and Endosomal Trafficking in
906 Plants. Annual review of plant biology 67:309-335. doi:10.1146/annurev-arplant-
907 043015-112242
908 Pirruccello M, Nandez R, Idevall-Hagren O, Alcazar-Roman A, Abriola L, Berwick SA, Lucast
909 L, Morel D, De Camilli P (2014) Identification of inhibitors of inositol 5-phosphatases
910 through multiple screening strategies. ACS Chem Biol 9 (6):1359-1368.
911 doi:10.1021/cb500161z
912 Platre MP, Jaillais Y (2016) Guidelines for the Use of Protein Domains in Acidic Phospholipid
913 Imaging. Methods in molecular biology 1376:175-194. doi:10.1007/978-1-4939-3170-
914 5_15
915 Platre MP, Noack LC, Doumane M, Bayle V, Simon MLA, Maneta-Peyret L, Fouillen L,
916 Stanislas T, Armengot L, Pejchar P, Caillaud MC, Potocky M, Copic A, Moreau P,
917 Jaillais Y (2018) A Combinatorial Lipid Code Shapes the Electrostatic Landscape of
918 Plant Endomembranes. Developmental cell 45 (4):465-480 e411.
919 doi:10.1016/j.devcel.2018.04.011
920 Posor Y, Eichhorn-Gruenig M, Puchkov D, Schöneberg J, Ullrich A, Lampe A, Müller R,
921 Zarbakhsh S, Gulluni F, Hirsch E (2013) Spatiotemporal control of endocytosis by
922 phosphatidylinositol-3, 4-bisphosphate. Nature 499 (7457):233-237
923 Posor Y, Eichhorn-Grünig M, Haucke V (2015) Phosphoinositides in endocytosis Molecular
924 and cell biology of lipids.
925 Rigal A, Doyle SM, Robert S (2015) Live cell imaging of FM4-64, a tool for tracing the endocytic
926 pathways in Arabidopsis root cells. Methods in molecular biology 1242:93-103.
927 doi:10.1007/978-1-4939-1902-4_9
928 Rivas MP, Kearns BG, Xie Z, Guo S, Sekar MC, Hosaka K, Kagiwada S, York JD, Bankaitis
929 VA (1999) Pleiotropic alterations in lipid metabolism in yeast sac1 mutants: relationship
930 to "bypass Sec14p" and inositol auxotrophy. Molecular biology of the cell 10 (7):2235-
931 2250. doi:10.1091/mbc.10.7.2235
932 Rodriguez-Furlan C, Minina EA, Hicks GR (2019) Remove, recycle, degrade: regulating
933 plasma membrane protein accumulation. The Plant cell 31 (12):2833-2854

934 Rodriguez-Villalon A, Gujas B, van Wijk R, Munnik T, Hardtke CS (2015) Primary root
935 protophloem differentiation requires balanced phosphatidylinositol-4,5-biphosphate
936 levels and systemically affects root branching. Development 142 (8):1437-1446.
937 doi:10.1242/dev.118364
938 Roy A, Levine TP (2004) Multiple pools of phosphatidylinositol 4-phosphate detected using
939 the pleckstrin homology domain of Osh2p. The Journal of biological chemistry 279
940 (43):44683-44689. doi:10.1074/jbc.M401583200
941 Schmid SL, Mettlen M (2013) Cell biology: Lipid switches and traffic control. Nature 499
942 (7457):161-162
943 Shin H-W, Hayashi M, Christoforidis S, Lacas-Gervais S, Hoepfner S, Wenk MR, Modregger
944 J, Uttenweiler-Joseph S, Wilm M, Nystuen A (2005) An enzymatic cascade of Rab5
945 effectors regulates phosphoinositide turnover in the endocytic pathway. The Journal of
946 cell biology 170 (4):607-618
947 Simon ML, Platre MP, Assil S, van Wijk R, Chen WY, Chory J, Dreux M, Munnik T, Jaillais Y
948 (2014) A multi-colour/multi-affinity marker set to visualize phosphoinositide dynamics
949 in Arabidopsis. The Plant journal : for cell and molecular biology 77 (2):322-337.
950 doi:10.1111/tpj.12358
951 Simon ML, Platre MP, Marques-Bueno MM, Armengot L, Stanislas T, Bayle V, Caillaud MC,
952 Jaillais Y (2016) A PtdIns(4)P-driven electrostatic field controls cell membrane identity
953 and signalling in plants. Nat Plants 2:16089. doi:10.1038/nplants.2016.89
954 Song L, Wang Y, Guo Z, Lam SM, Shui G, Cheng Y (2021) NCP2/RHD4/SAC7, SAC6 and
955 SAC8 phosphoinositide phosphatases are required for PtdIns4P and PtdIns (4, 5) P2
956 homeostasis and Arabidopsis development. New Phytologist
957 Takagi J, Uemura T (2018) Use of Brefeldin A and Wortmannin to Dissect Post-Golgi
958 Organelles Related to Vacuolar Transport in Arabidopsis thaliana. Methods in
959 molecular biology 1789:155-165. doi:10.1007/978-1-4939-7856-4_12
960 Tejos R, Sauer M, Vanneste S, Palacios-Gomez M, Li H, Heilmann M, van Wijk R, Vermeer
961 JE, Heilmann I, Munnik T, Friml J (2014) Bipolar Plasma Membrane Distribution of
962 Phosphoinositides and Their Requirement for Auxin-Mediated Cell Polarity and
963 Patterning in Arabidopsis. The Plant cell 26 (5):2114-2128.
964 doi:10.1105/tpc.114.126185
965 Terebiznik MR, Vieira OV, Marcus SL, Slade A, Yip CM, Trimble WS, Meyer T, Finlay BB,
966 Grinstein S (2002) Elimination of host cell PtdIns(4,5)P(2) by bacterial SigD promotes
967 membrane fission during invasion by Salmonella. Nature cell biology 4 (10):766-773.
968 doi:10.1038/ncb854
969 Thole JM, Vermeer JE, Zhang Y, Gadella TW, Jr., Nielsen E (2008) Root hair defective4
970 encodes a phosphatidylinositol-4-phosphate phosphatase required for proper root hair
971 development in Arabidopsis thaliana. The Plant cell 20 (2):381-395.
972 doi:10.1105/tpc.107.054304
973 van Leeuwen W, Vermeer JE, Gadella TW, Jr., Munnik T (2007) Visualization of
974 phosphatidylinositol 4,5-bisphosphate in the plasma membrane of suspension-
975 cultured tobacco BY-2 cells and whole Arabidopsis seedlings. The Plant journal : for
976 cell and molecular biology 52 (6):1014-1026. doi:10.1111/j.1365-313X.2007.03292.x
977 Vollmer AH, Youssef NN, DeWald DB (2011) Unique cell wall abnormalities in the putative
978 phosphoinositide phosphatase mutant AtSAC9. Planta 234 (5):993-1005.
979 doi:10.1007/s00425-011-1454-4
980 Wickham H (2016) ggplot2: elegant graphics for data analysis. springer,
981 Williams ME, Torabinejad J, Cohick E, Parker K, Drake EJ, Thompson JE, Hortter M, Dewald
982 DB (2005) Mutations in the Arabidopsis phosphoinositide phosphatase gene SAC9
983 lead to overaccumulation of PtdIns(4,5)P2 and constitutive expression of the stress-
984 response pathway. Plant physiology 138 (2):686-700. doi:10.1104/pp.105.061317
985 Yan X, Wang Y, Xu M, Dahhan DA, Liu C, Zhang Y, Lin J, Bednarek SY, Pan J (2021) Cross-
986 Talk between Clathrin-Dependent Post-Golgi Trafficking and Clathrin-Mediated
987 Endocytosis in Arabidopsis Root Cells. The Plant cell

988 Yoshida S, Ohya Y, Goebl M, Nakano A, Anraku Y (1994) A novel gene, STT4, encodes a
989 phosphatidylinositol 4-kinase in the PKC1 protein kinase pathway of Saccharomyces
990 cerevisiae. The Journal of biological chemistry 269 (2):1166-1172
991 Yperman K, Papageorgiou AC, Merceron R, De Munck S, Bloch Y, Eeckhout D, Jiang Q, Tack
992 P, Grigoryan R, Evangelidis T (2021a) Distinct EH domains of the endocytic TPLATE
993 complex confer lipid and protein binding. Nature communications 12 (1):1-11
994 Yperman K, Wang J, Eeckhout D, Winkler J, Dai Vu L, Vandorpe M, Grones P, Mylle E, Kraus
995 M, Merceron R (2021b) Molecular architecture of the endocytic TPLATE complex.
996 Science Advances 7 (9):eabe7999
997 Zhang Y, Persson S, Hirst J, Robinson MS, van Damme D, Sanchez-Rodriguez C (2015)
998 Change your TPLATE, change your fate: plant CME and beyond. Trends in plant
999 science 20 (1):41-48. doi:10.1016/j.tplants.2014.09.002
1000 Zhao Y, Yan A, Feijo JA, Furutani M, Takenawa T, Hwang I, Fu Y, Yang Z (2010)
1001 Phosphoinositides regulate clathrin-dependent endocytosis at the tip of pollen tubes in
1002 Arabidopsis and tobacco. The Plant cell 22 (12):4031-4044.
1003 doi:10.1105/tpc.110.076760
1004 Zhong R, Burk DH, Morrison WH, 3rd, Ye ZH (2004) FRAGILE FIBER3, an Arabidopsis gene
1005 encoding a type II inositol polyphosphate 5-phosphatase, is required for secondary
1006 wall synthesis and actin organization in fiber cells. The Plant cell 16 (12):3242-3259.
1007 doi:10.1105/tpc.104.027466
1008 Zhong R, Burk DH, Nairn CJ, Wood-Jones A, Morrison WH, 3rd, Ye ZH (2005) Mutation of
1009 SAC1, an Arabidopsis SAC domain phosphoinositide phosphatase, causes alterations
1010 in cell morphogenesis, cell wall synthesis, and actin organization. The Plant cell 17
1011 (5):1449-1466. doi:10.1105/tpc.105.031377
1012 Zhong R, Ye ZH (2003) The SAC domain-containing protein gene family in Arabidopsis. Plant
1013 physiology 132 (2):544-555. doi:10.1104/pp.103.021444
1014 Zhuang X, Wang H, Lam SK, Gao C, Wang X, Cai Y, Jiang L (2013) A BAR-domain protein
1015 SH3P2, which binds to phosphatidylinositol 3-phosphate and ATG8, regulates
1016 autophagosome formation in Arabidopsis. The Plant cell 25 (11):4596-4615.
1017 doi:10.1105/tpc.113.118307
1018